HIGH ENERGY LASER POINTING THROUGH EXTENDED TURBULENCE

THESIS

Jason A. Tellez, Captain, USAF

AFIT/GE/ENG/02-31

DEPARTMENT OF THE AIR FORCE
AIR UNIVERSITY

AIR FORCE INSTITUTE OF TECHNOLOGY

Wright-Patterson Air Force Base, Ohio

The views expressed in this thesis are those of the author and do not reflect the official policy or position of the United States Air Force, Department of Defense, or the United States Government.

AFIT/GE/ENG/02-31

HIGH ENERGY LASER POINTING THROUGH EXTENDED TURBULENCE

THESIS

Presented to the Faculty
Department of Computer and Electrical Engineering
Graduate School of Engineering and Management
Air Force Institute of Technology
Air University
Air Education and Training Command
in Partial Fulfillment of the Requirements for the
Degree of Master of Science in Electrical Engineering

Jason A. Tellez, B.S.
Captain, USAF

September, 2002

AFIT/GE/ENG/02-31

HIGH ENERGY LASER POINTING THROUGH EXTENDED TURBULENCE

Jason A. Tellez, B.S.

Captain, USAF

Approved:

	6 Sep 02
Maj Eric P. Magee Ph.D. Thesis Advisor	Date
Peter S. Maybeck	6 Sep 02
Dr. Peter S. Maybeck Committee Member	Date
M. Pachter	6 Sept 02
Dr. Meir N. Pachter Committee Member	Date

Acknowledgments

I would like to thank my friends, family and colleagues that have supported me in this work. I would like to thank Major Magee, Dr. Peter Maybeck, and Dr. Meir Pachter for helping with my thesis. I would specifically like to thank Major Magee for putting up with my continual delays in finishing this effort.

I reserve special thanks to my wife for encouraging me, supporting me, and putting up with long one-sided talks about what I happen to be working on that day.

Finally, it is always with great pleasure that I have been able study the marvellous details of God's creation. "For since the creation of the world His invisible attributes are clearly seen, being understood by the things that are made ... so that they are without excuse." (Romans 1:20) Even more so for the scientist.

Jason A. Tellez

Table of Contents

List of Figures

Abstract

The airborne laser (ABL) uses adaptive optics to compensate for the atmospheric turbulence between the ABL and the target. The primary purpose of this compensation is to increase the energy density of the high energy laser at the target. However, the specifics of the engagement scenario require the tracking point of reference and the adaptive optics point of reference to be located at different points on the target.

This research considers the effects of tracking a target in one direction while compensating for atmospheric turbulence in a different direction. The target references used are a point source and a rectangle, while a point source alone is used for the adaptive optics reference. It will be shown that compensating for atmospheric turbulence in a different direction than tracking results in a bias in the mean tracking error while having no appreciable affect on track jitter.

HIGH ENERGY LASER POINTING THROUGH EXTENDED TURBULENCE

I. Introduction

1.1 Problem Statement

The introduction of the laser brought with it promises of Buck Rogers and Star Wars. Few would have thought that the largest impact would have been in how we listen to music or watch movies. However, developments in high powered lasers and beam control have revived those old promises. These new weapons, such as the Airborne Laser (ABL), seek to focus megawatts of laser energy on a target hundreds of kilometers away.

Accomplishing this impressive task involves solving several different problems. The first and most obvious entails developing a laser source powerful enough to produce megawatts of laser energy. After that, the energy needs to be delivered accurately to the target. A more subtle problem involves ensuring that the laser energy, when it reaches the target, is of the best quality possible using a technique known as adaptive optics. Difficulties may arise when the tracking and pointing becomes dependent on the performance of the adaptive optics. In the case of the ABL, the tracking reference (i.e., the nose of the missile) is separated from the adaptive optics reference. This spatial separation causes light from both sources to travel different paths. The purpose of this research is to determine the effect on tracking using an adaptive optics reference that is not co-located with the tracking reference.

1.2 Scope

Previous work [6, 7] examined the effects of spatially separated paths on tracking alone or adaptive optics as a whole. This work is extended by tracking solely along one path and compensating for higher order distortions along another path. Performance is determined by sending a scoring beam back through the atmosphere to the target. The adaptive optics algorithm used is a straightforward least squares reconstructor [14], which provides the necessary contrast to an uncompensated image.

1.3 Thesis Organization

Chapter two contains background information on the ABL, adaptive optics, and image tracking. The ABL is considered first, concentrating on the geometry of a typical ABL engagement and the optical system layout. An overview of adaptive optics as it relates to this research follows. Lastly, a few tracking techniques are broken down, specifically the centroid and edge tracking algorithms. Their advantages and disadvantages are discussed, as well as what can be done with them.

Chapter three looks at the specific methodology used for determining the performance of the systems. First, the effects of anisoplanatic compensation are examined theoretically. Then, the simulation itself is discussed in all of its aspects.

Chapter four examines and interprets the results of the simulation work. This includes validation of the technique as well as results from the tracking experiments themselves. It also includes the techniques used to examine the results and how to interpret them.

In Chapter five, the conclusions are discussed and avenues for future research are proposed.

II. Background

2.1 Introduction

Adaptive optics has been used extensively in various applications including astronomical imaging, laser beam propagation, and even within the laser resonators themselves [3, 5, 14, 15]. This thesis looks at a particular form of the anisoplanatic [6] problem of adaptive optics and how it relates to the Airborne Laser (ABL). The discussion begins with a description of the ABL engagement scenario and system layout. This is followed by a brief overview of adaptive optics. This will include a general description of adaptive optics architecture, some limitations imposed by the atmosphere, and how tracking is separated from the higher order correction. A discussion of various tracking algorithms follows. Finally a description of the specific problem at hand will tie together the previous sections of this chapter.

2.2 The Airborne Laser

The ABL is an aircraft designed for short range ballistic missile defense. It consists of a chemical oxygen iodine laser (COIL) inside a Boeing 747 with a 1.5 meter diameter turret mounted on the nose (Figure 2.1).

Figure 2.1. Artistic rendition of the Airborne Laser.

In addition to the COIL, three other lasers are critical to system operation. The first is the Active Ranger System, which provides precise range data for tracking.

The next laser is the track illuminator laser (TILL). The TILL flood illuminates the nose of the missile with enough energy to produce a return. The returning light allows the ABL to determine the precise position of the nose of the missile, providing a reference from which all of the remaining lasers are aimed. The third laser is the beacon illuminator laser (BILL). The BILL is aimed down the body of the missile and provides the reference for the adaptive optics. Lastly the COIL is located further down the body of the missile. The entire setup is shown in Figure 2.2.

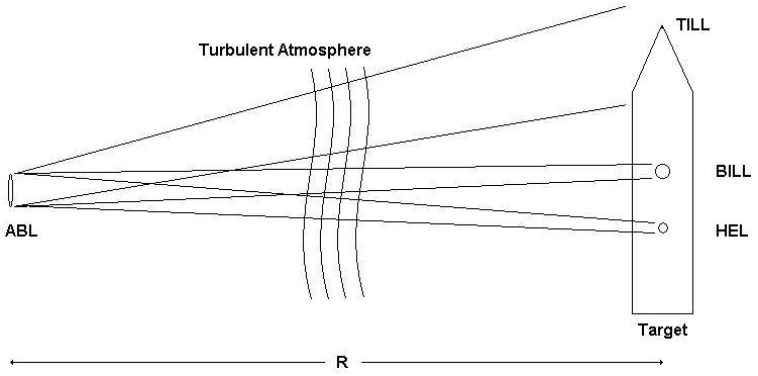

Figure 2.2. ABL engagement scenario.

The separation between the placement of the BILL on the missile and the placement of the high energy laser (HEL) COIL is fixed at $(2R/c + \Delta t)\, v$. Here R is the range between the ABL and the target, c is the speed of light, Δt is the sum total of any latencies in the ABL beam control system, and v is the transverse velocity of the missile relative to the ABL. This distance is fixed so that the HEL travels through the exact same path that the reflection of the BILL from the missile travelled. Therefore, in order to hit a desired spot on the missile, the BILL aimpoint must be adjusted [2].

It is also important to note that the TILL, BILL, and HEL all pass through the same aperture and beam control system. This means that any correction applied as a result of the tracking system, which is based on TILL return, effects the BILL

and HEL. Also, any adaptive optics correction applied, which is based on the BILL return, effects the TILL and HEL also.

2.3 Adaptive Optics Overview

Adaptive optics involves compensating a beam of light for distortions that may have occurred during propagation. Using some sort of reference, ideally a point source located at the object to be imaged, the distortions experienced by the reference can be compared to what the reference would have looked like without the distortions. Once these differences are known, action can be taken to reverse them. Assuming light from the object travels the same path in the same way as the reference, these actions improve the quality of the image of the object.

2.3.1 Adaptive Optics Architecture. An adaptive optics systems can be broken into three very basic elements: the wavefront sensor, the reconstructor, and the wavefront corrector.

1. Wavefront Sensor

   The wavefront sensor is the device used to measure the optical phase of the light received from the reference. There are many ways to measure the incident phase at varying degrees of complexity. Wavefront sensors can be divided into two basic classes: image plane sensors and aperture plane sensors [9].

   Image plane sensors, or single intensity detectors, attempt to maximize the intensity of the image of the reference. The simplest method uses a single detector to measure an image sharpness function such as:

$$S = \int I(x,y)M(x,y)dxdy \tag{2.1}$$

   where $I(x,y)$ is the reference intensity at the image plane and $M(x,y)$ is some masking function such as a pinhole. The detector then measures the total light

passing through the mask, which is maximized when the optical system is free from aberration [9].

Aperture plane sensors attempt to measure the wavefront of the incoming beam. There are several methods to do this, including Hartmann sensors and shearing interferometers [9]. A Hartmann wavefront sensor images the pupil of the optical system. By using a lenslet array of n by n lenses, the pupil is broken up into n^2 small images, or subapertures, on a detector (shown in Figure 2.3). The wavefront sensor then calculates the position of the spot in each subaperture, and uses the resulting slopes to calculate the wavefront gradient which is used to reconstruct the wavefront.

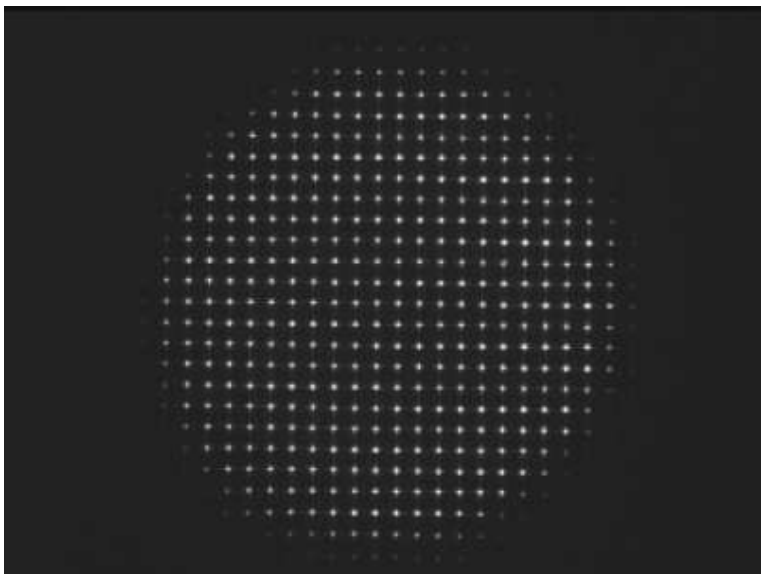

Figure 2.3. Hartmann wavefront sensor showing the image seen at the detector plane, an array of spots fromed by the lenslet array [10].

2. The Reconstructor

Once the measurements are made by the wavefront sensor, the actual wavefront must be reconstructed. This is done by the wavefront reconstructor. Once common way to reconstruct the wavefront, and the method used in this research, is to use a least squares reconstructor [14]. The least squares reconstruction

matrix is defined by

$$M = \left(H^T H\right)^{-1} H^T \tag{2.2}$$

H is the Jacobian matrix such that the equation

$$s_m = Hc \tag{2.3}$$

is satisfied. Here s_m is a column vector containing the measured slopes from the wavefront sensor, and c is a column vector of control signals. An important note on the least square reconstructor is that neither atmospheric statistics nor noise statistics are required. This simplicity makes it the most used technique in current adaptive optics systems [14].

3. Wavefront Corrector

The wavefront corrector is a device that can alter the wavefront characteristics of the incoming wave. Correctors can be classed as either modal or zonal. Modal correctors correct specific abberations. These abberations are typically described using the Zernike polynomials [12] defined by

$$\left.\begin{aligned} Z_{evenj} &= \sqrt{n+1} R_n^m(r)\sqrt{2}\cos m\theta \\ Z_{oddj} &= \sqrt{n+1} R_n^m(r)\sqrt{2}\sin m\theta \end{aligned}\right\} \quad m \neq 0$$
$$Z_j = \sqrt{n+1} R_n^0(r) \qquad m = 0 \tag{2.4}$$

where

$$R_n^m = \sum_{s=0}^{(n-m)/2} \frac{(-1)^s (n-2)!}{s!\left[(n+m)/2-s\right]!\left[(n-m)/2-s\right]!} r^{n-2s} \tag{2.5}$$

The values of n and m are always integers and satisfy $m \leq n$ and $n - |m| = even$. The index j is used to denote mode ordering and is a function of n and m. The Zernike polynomials are typically used in the expansion of the wavefront over a circular aperture of radius R. If $\phi(r,\theta)$ represents the wavefront then

the polynomial expansion over a circle of radius R is given by

$$\phi(R\rho,\theta) = \sum_j a_j Z_j(\rho,\theta) \tag{2.6}$$

where $\rho = r/R$ and the coefficents a_j are given by

$$a_j = \int \mathrm{d}\rho W(\rho)\,\phi(R\rho,\theta)\,Z_j(\rho,\theta) \tag{2.7}$$

where $W(\rho)$ is the pupil function. This allows the wavefront to be described in terms of the Zernike polynomials, for instance the X tilt and Y tilt components are defined by the Zernike polymonials $Z_2 = 2r\cos\theta$ and $Z_3 = 2r\sin\theta$ respectively, defocus described by $Z_4 = \sqrt{3}(2r^2 - 1)$, and so on. $Z_1 = 1$, referred to as piston, is unobservable and has no effect on the image. A modal corrector then only compensates for particular abberations, such as tilt and defocus.

Zonal correctors break the wavefront into pieces and apply the necessary correction to each piece [15]. A zonal corrector works well with a Hartmann wavefront sensor, in that each subaperture can be fitted to each zone of the zonal corrector.

2.3.2 Atmospheric Limitations. Light passing through any inhomogeneous medium becomes distorted. In the case of the atmosphere, these distortions are caused by minute variations in the index of refraction along the beam's path. These variations are ultimately caused by temperature fluctuations resulting in density changes.

The turbulence characteristics of a given path through the atmosphere is commonly characterized by the parameters r_0 and θ_0. The parameter r_0 is known as the *atmospheric coherence length* or *Fried parameter* [6]. This number gives an effective

diameter of the system if there were no atmosphere present. The expression for r_0 is

$$r_0 = \left\{ (2.905/6.88)\, k^2 \int_0^L dz C_N^2(z) \left[1 - (z/L)\right]^{5/3} \right\}^{-3/5} \tag{2.8}$$

Here k is the wave number defined by $2\pi/\lambda$, L is the path length, C_N^2 is the index of refraction structure constant, and z is the integration variable along the path. Assumptions are that there is spherical wave propagation and the turbulence follows the Kolmogorov spectrum [15] defined by

$$\Phi_n(K) = 0.033 C_n^2 K^{-11/3} \tag{2.9}$$

where Φ_n is the power spectral density and K is the three-dimensional spatial wave number.

The parameter θ_0 defines the isoplanatic angle. This angle determines the angle within which the adaptive optics beacon and the object to be imaged must exist relative to the observer, outside of which the paths are uncorrelated. Once the beacon and object are separated by more than this angle, the corrections applied by the adaptive optics systems begins to have an overall degrading effect on the image of the object. The parameter θ_0 is described by the equation

$$\theta_0 = \left\{ 2.905 k^2 \int_0^L dz C_N^2(z) z^{5/3} \right\}^{-3/5} \tag{2.10}$$

and makes the same assumptions as r_0 [6].

2.3.3 Tracking as a Separate Problem. Over 86% of the total wavefront error is due to the tilt component of the atmosphere [14]. Since wavefront correctors, such as deformable mirrors, have small dynamic range, tilt is usually corrected by using a fast steering mirror (FSM). Since tilt can be measured from a single image using the entire aperture, the problem boils down to simply tracking the center of

the reference, assuming the reference is a point source. In most cases, the object to be imaged is not a point source, but some other adaptive optics reference exists, or can be made, within the isoplanatic angle of the object. In these instances, it is desirable to track the object and not the reference.

When tilt is corrected using a separate system, it becomes necessary not to correct for tilt using the adaptive optics portion of the system (i.e., the wavefront sensor and corrector). When this is done, the wavefront is reconstructed from the wavefront sensor with no overall X or Y tilt. This is also know as tilt-removed reconstruction.

2.4 Tracking Algorithms

Tracking algorithms can be broken down into two basic forms, centroid trackers and feature trackers. The following equations are the definition of a centroid:

$$\bar{x} = \int\int I(x,y)\, x \,\mathrm{d}x\,\mathrm{d}y \Big/ \int\int I(x,y)\,\mathrm{d}x\,\mathrm{d}y \tag{2.11}$$

$$\bar{y} = \int\int I(x,y)\, y \,\mathrm{d}x\,\mathrm{d}y \Big/ \int\int I(x,y)\,\mathrm{d}x\,\mathrm{d}y \tag{2.12}$$

where I is the intensity at the image plane of the receiver. Feature trackers attempt to match the image to some reference map. This technique ranges in complexity from a simple edge tracker to a full blown correlation tracker.

2.5 The Problem

The specific problem examined looks at the implications of tracking an object in one direction, while compensating for everything but tilt in another direction. Figure 2.4 shows a skeleton of the simulation experiment. P_1 and P_2 represent point sources, the tracking beacon and the adaptive optics beacon respectively, at the target plane, which are separated by Δx. For the extended source simulations, the tracking beacon is replaced by an extended beacon with a center of mass located at

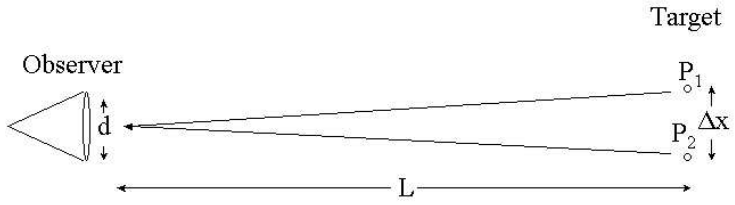

Figure 2.4. Schematic of the basic problem. The target represents two point sources at different locations at the target plane. For the extended source simulations, one of the point sources is replaced with an extended object.

P_1 such that Δx is the difference between the center of the target and the adaptive optics beacon.

The simulation uses a Hartmann wavefront sensor with 128 x 128 subapertures and a least squares estimator with the tilt components removed. The wavefront corrector uses an optical phase delay at the same grid level as the wavefront sensor [16]. A centroid tracker is placed at the image plane for tilt control. Performance is determined by compensating a scoring beam using the tilt commands from the tracker and sending the beam to a target board (an array of sensors spaced 1cm apart) located at the target plane. The tracking beacon, whether a point source or extended, is always located at the center of the target board. Further details will be discussed in Chapter 3.

2.6 Summary

This chapter introduced several principles that will be referenced in the following chapters. First, the operation of the Airborne Laser was discussed. This was followed by a discussion of adaptive optics. The adaptive optics section reviewed the basic architecture of a generic system and some basic principles of operation. This was followed by a discussion on the limitations that the atmosphere imposes on adaptive optics systems. Next, tracking was discussed, focusing on the centroid

tracker and how it is used. Finally, a discussion of the problem to be researched was presented.

III. Methodology

3.1 Introduction

As discussed before, this research investigates a particular aspect of anisoplanatism. The experiment is done entirely using wave optics simulation.

3.2 Analysis

Beginning with the equations for r_0 and θ_0, these can be further simplified assuming a constant altitude resulting in a constant C_N^2. The results from Fried [6] are

$$r_0 = 3.02k^{-6/5}L^{-3/5}\left(C_N^2\right)^{-3/5} \tag{3.1}$$

and

$$\theta_0 = 0.950k^{-6/5}L^{-8/5}\left(C_N^2\right)^{-3/5} \tag{3.2}$$

k is the wave number and L is the path length. The simulation is actually given r_0 to generate the turbulence so that

$$\theta_0 = \frac{0.950}{3.02}\frac{r_0}{L} \tag{3.3}$$

The simulation uses a constant altitude for two primary reasons. First, it simplifies the relationship between the turbulence level in the simulation, i.e. r_0, and the isoplanatic angle. Second, it closely resembles a real world experimental setup at the North Oscura Peak (NOP) facility at White Sands Missile Range [1]. This facility consists of a 1.0 meter (m) telescope, with associated tracking and adaptive optics systems, located on a mountain peak at an altitude of approximately 2400m. A second station at Salinas peak, nearly 50 kilometers (km) away provides a stationary target, which can be used by the facilities at NOP for tests.

3.3 Simulation Method

The simulation used the wave optics package WaveTrain^{TM} [11]. The simulation uses two dimensional meshes of complex numbers to represent the propagating beam(s) of light [4]. For propagation of the complex meshes, WaveTrain uses the Fast Fourier Transform technique base on the Fresnel diffraction integral [8]:

$$U(x,y) = \frac{e^{jkz}}{j\lambda z} e^{j\frac{k}{2z}\left(x^2+y^2\right)} \int_{-\infty}^{\infty}\int_{-\infty}^{\infty} \left\{ U(\xi,\eta)\, e^{j\frac{k}{2z}\left(\xi^2+\eta^2\right)} \right\} e^{-j\frac{2\pi}{\lambda z}(x\xi+y\eta)} d\xi d\eta \qquad (3.4)$$

where: x and y represent the coordinates at the output plane, ξ and η represent the coordinates at the input plane, and z is the propagation distance.

The simulation used is comprised of three major subsystems: the target, the atmosphere, and the observer, as shown in Figure 3.1. Each subsystem contains various components of the simulation such as sources, detectors, and other optical subsystems. Figure 3.1 also shows the lines connecting the subsystems together, representing which components share information and in what direction. In this case, each connection shows a two-way relationship, meaning data is sent in both directions along the connection. Also, blocks are given two names. The first name, which is always capitalized, describes the block's C++ class. The second name, in all lowercase letters, defines an instance of the class that defines the block. Wavetrain uses the graphical interface to define relationships between subsystems, which is used to then generate C++ source code, which is compiled and executed for each simulation run.

3.3.1 The Target. The target subsystem, shown in Figure 3.2, consists of the target board, the target, and the adaptive optics reference. The large arrows in Figure 3.2 represent the light coming into the target subsystem. The labels *incomingTransmitted* and *outgoingIncident* represent the light leaving the target block and entering the target block respectively. Incoming is defined as light moving from

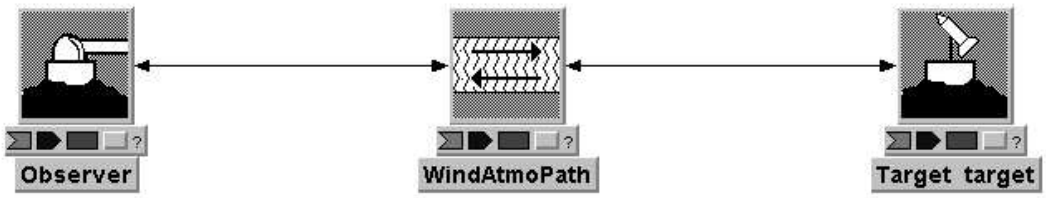

Figure 3.1. Overall system layout.

right to left, and outgoing is defined as light moving from left to right. An easy way to remember is that everything is defined from the point of view of the HEL on the ABL.

Starting with the *outgoingIncident* arrow, the light is sent to an *IncomingCombiner* block. This block allows for two sources to be combined for transmittance in one direction, while the other direction just allows one beam to pass. The light from the *outgoingIncident* arrow passes through the *IncomingCombiner* block unmodified and is sent to the target board. From the other direction, the light from the *PointSource* block and the *incoherentreflector* block are combined and sent to the *incomingTransmitted* arrow and out the Target subsystem.

3.3.1.1 Target Board. The target board consists of a grid of 256 by 256 sensors, which will be the propagation grid of the simulation. Each sensor is 1 cm wide and is sensitive only light to with a wavelength of 1 μm, the wavelength of the HEL. 1 μm was used as the center wavelength of the simulation since it is the same wavelength used at the NOP facility. The target board feeds a centroid calculator, the results of which are stored for post-processing. Additionally, the images of the target board can be recorded.

3.3.1.2 The Target. The target shown in Figure 3.2 consists of an incoherent reflector and a uniform illuminator. The reflector consists of a 32 pixel tall

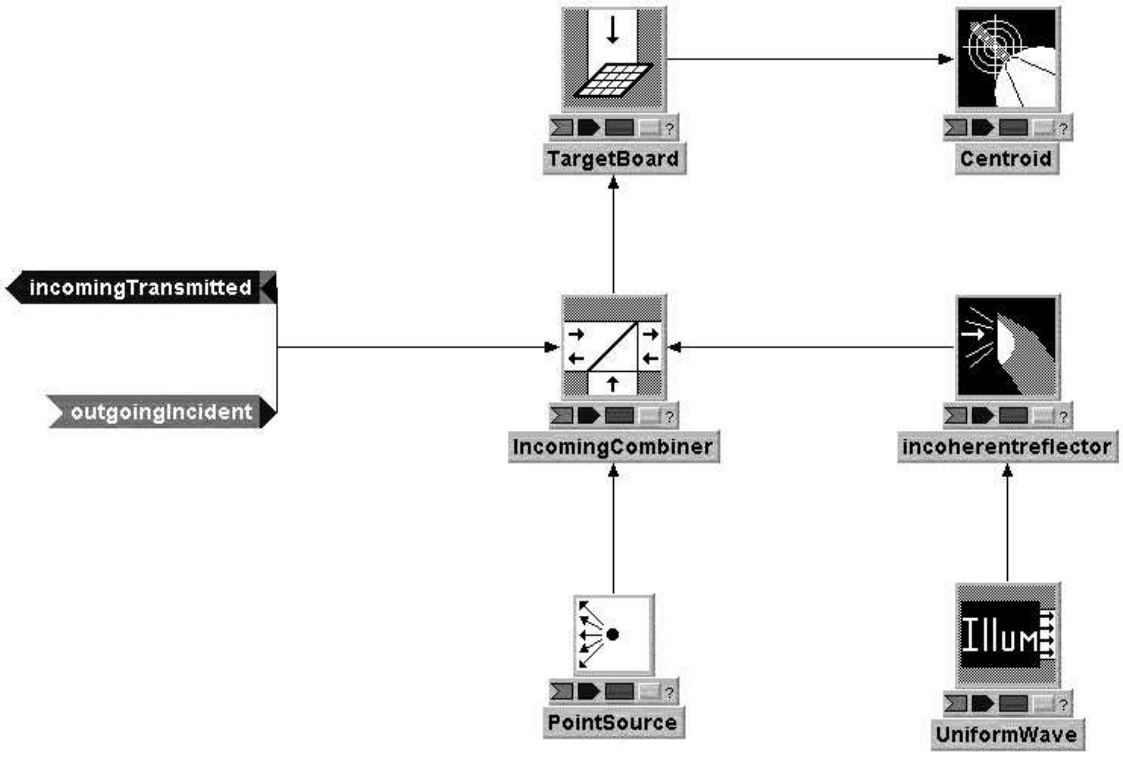

Figure 3.2. Target subsystem layout.

by 16 pixel wide array. The incoherent reflector acts as a light scattering device, with no coherence to the spatial properties of light reflected. Eight random realizations were used to produce each incoherent reflection pattern. The uniform illuminator simply flood illuminates the incoherent reflector with 1.001 μm wavelength light. The array is centered on the the center of the target board. For the point source tracking portion of the experiment, the incoherent reflector and the uniform illuminator are replaced by a point source centered on the target board. This takes the place of the TILL on the ABL.

3.3.1.3 The Adaptive Optics Reference. This experiment used a point source for the adaptive optics reference. The source has a wavelength of 0.999 μm and can be placed anywhere on the target board. This experiment holds the source

at the vertical center of the target board and moves along the horizontal axis. This takes the place of the BILL on the ABL.

The main reason different wavelengths were chosen for the sources was to allow the sensors in the simulation to discriminate between them, thus only a 0.001 μm difference. Also, by placing all of the sources at the target end of the simulation, they represent ideal illumination. In the case of the ABL, the BILL and TILL are distorted by the atmosphere before they reach the target. In this simulation this is not the case. This was done to isolate the anisoplanatic effects from any that might arise due to the outgoing distortion of the BILL or TILL.

3.3.2 The Atmosphere. The atmosphere is modelled using several discrete thin phase screens place along the path between the target and the observer. A thin phase screen simulates the atmosphere by generating a grid such that

$$U(x,y) = U_0(x,y)\, T_s(x,y) \tag{3.5}$$

where U_0 is the input field, U is the output field, and T_s is the transparency function describing the random field perturbation due to the atmosphere [14]. Thin phase screens are useful in wave optics simulations, in that an entire random segment of atmosphere can be reduced to one simple relation, vastly reducing computation time. This particular simulation used a propagation length of 50km with 5 phase screens evenly spaced along the path. The number of phase screens was chosen based on the rule of thumb that dictates one phase screen for every 10km of propation.

Figure 3.3 shows the internals of the Atmosphere subsystem. The incoming light follows a path from the top right arrow, labeled *WaveTrain*, to the bottom left arrow. The outgoing light goes from the top left arrow to the bottom right arrow. The *TransverseVelocity* blocks allow for the addition of the simulation of wind. It does this by "sliding" the phase screens, which are contained in the *AtmoPath*

block, across the path. This simulation does not contain any wind velocity, thus the atmosphere is "frozen" for the duration of each run.

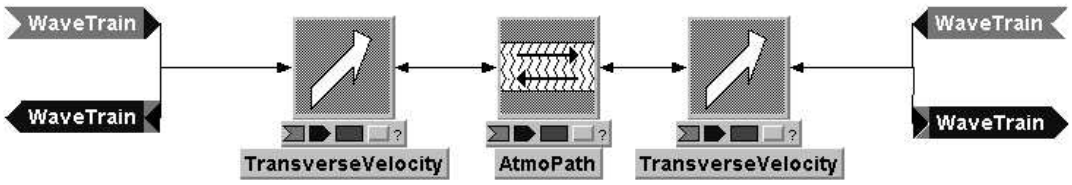

Figure 3.3. Atmospheric turbulence block.

3.3.3 The Observer. The observer block consists of several subcomponents. Overall, it consists of four cameras with centroid detectors, the adaptive optics compensation, the outgoing steering mirror, and the scoring laser. Starting from the bottom right of Figure 3.4, the light enters the telescope block. The telescope has diameter of .5m with no annulus and focused on the target, 50km away. The telescope therefore collimates the light from that point on back. The incoming light then passes through the *OutgoingCombiner* block and proceeds to a beamsplitter. This splits the beam into two nearly identical paths, the difference being that one path has a compensator and the other does not. The output of both of the camera blocks are tilt commands that are sent to a selector. The selector determines which one of the four cameras will control the beam steering mirror. The four cameras represent the compensated TILL image, uncompensated TILL image, compensated BILL image, and uncompensated BILL image. Only one camera is allowed to control the steering mirror at a time so that comparisons can be made between the performance of the different cameras. The selector is designed so that tilt commands can be combined between the cameras if desired. The scoring laser (shown as the bottom left block) is sent to the steering mirror, through the telescope, and out to the target board.

One important aspect of the observer is the limitation of the steering mirror. The simulation allows for the steering mirror to have an instantaneous response to the

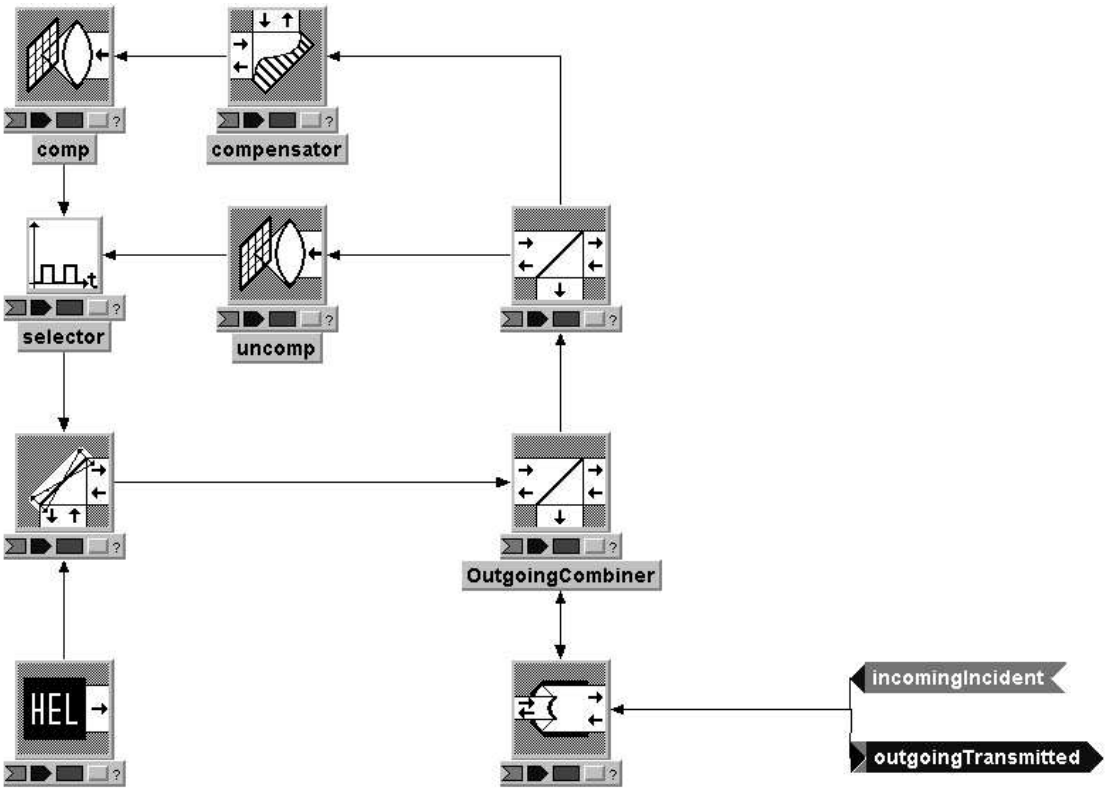

Figure 3.4. Observer block.

commanded input. However, the light takes one time step to propagate. Therefore, in the first time step, the light propagates from the target to the observer. In the next time step, the cameras calculate the centroids and the command is sent to the steering mirror. In the third time step the mirror reaches its final position, taking only the one time step to do so. Finally, in the fourth time step the light from the HEL is propagated to the target board, after having been redirected by the steering mirror. In all, 4 time steps are required, not for the simulation of wind or any other temporal effects of the atmosphere, but to allow the control elements to reach their final state and for the light to propagate.

3.3.3.1 The Compensator. Figure 3.5 shows the adaptive optics compensation block. Following the light in from the right, the incoming beam is split. The first path, to the left, is again split between a beam steering mirror and a camera. The camera is sensitive only to the wavelength of the the adaptive optics beacon. The camera outputs an intensity map to the centroid calculator, which outputs x and y tilts. These tilts are inverted and sent as commands to the *BeamSteeringMirror* block, with a time constant of 1 μs. This process removes the tilt from the beam coming from the second beam splitter, thus producing a tilt-removed reconstructor while still using a simple least squares reconstructor.

After the tilt has been removed, the field is sent to a *SimpleFieldSensor* block. This block, just as the name implies, senses the field at the grid level. The resulting values are sent to the reconstructor block. This reconstructor was written entirely in Matlab® by Jeff Barchers and Brent Ellerbrook from the Air Force Research Laboratory, Starfire Optical Range and modified for WaveTrain by Virgil Zetterlind [16]. It implements the least squares algorithm discussed in Chapter 2. The reconstructor outputs commands to an optical phase delay map, that acts on the original incoming beams (both the TILL and BILL returns), thereby compensating the beam.

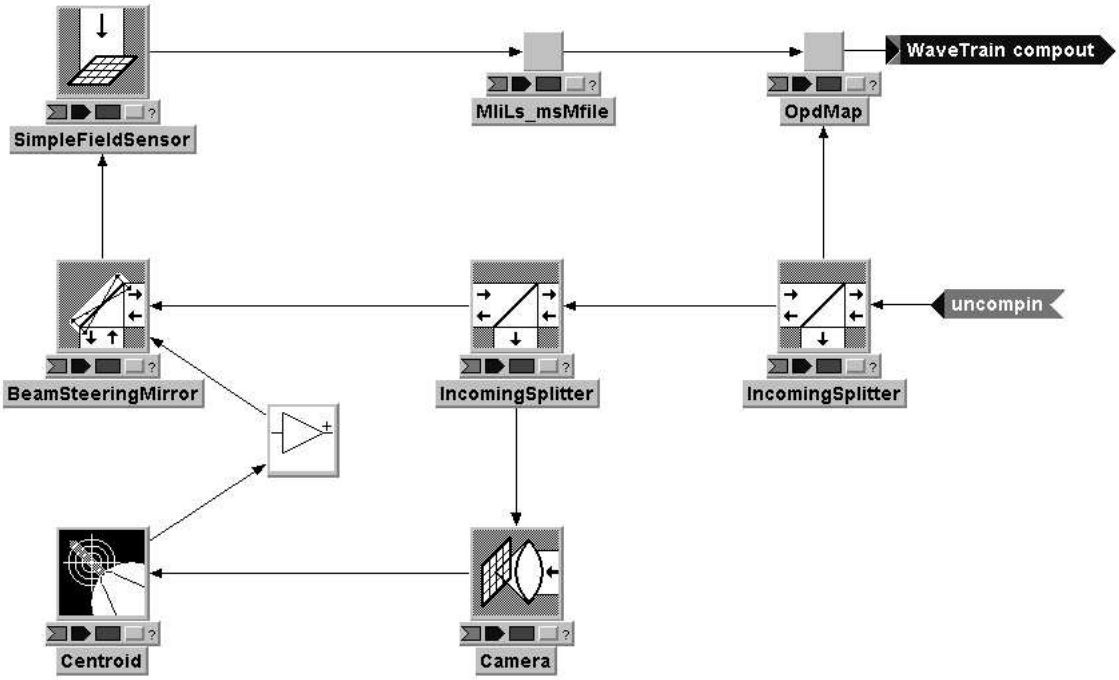

Figure 3.5. Compensator block.

3.3.3.2 The Cameras. The camera blocks, shown in Figure 3.6 and labeled *comp* and *uncomp* in Figure 3.4 , are identical to each other with the exception of their inputs. One receives the beam unmodified after the telescope while the other receives the beam after it has been compensated for higher order (other than tilt) aberrations. In both camera blocks, the top sensor is tuned only to the track beacon, while the bottom is tuned to the adaptive optics beacon. The outputs of the subsystem are the centroids from the two sensors.

3.3.3.3 The Control Selector. The last subsystem within the observer is the control selector block. In this block, the centroid calculation from the two camera blocks (totalling four in all: uncompensated track beacon, uncompensated adaptive optics beacon, compensated track beacon, and compensated adaptive optics beacon) are multiplied by some gain and then summed together. By toggling the gain at runtime between 0 and 1, the camera that controls the scoring laser steering mirror can be chosen. For example, by setting the gains to {1,0,0,0} the uncompensated

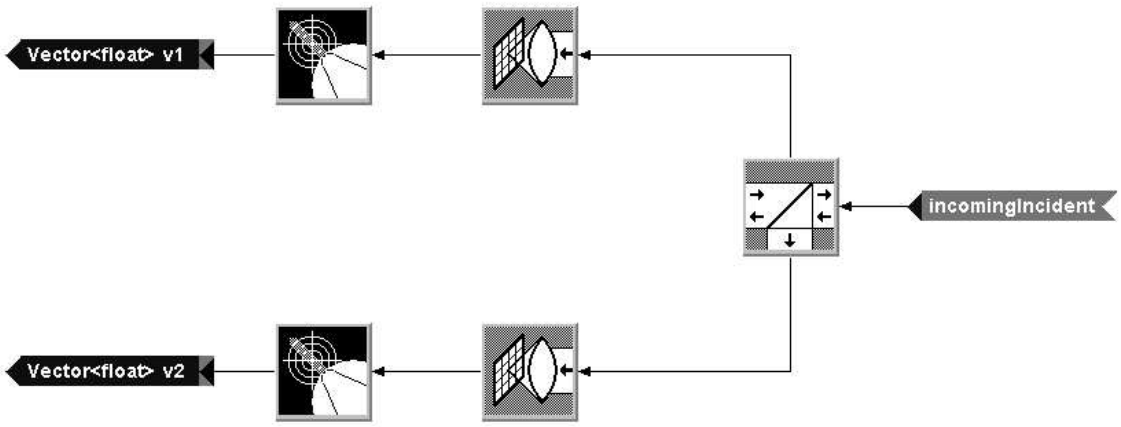

Figure 3.6. Camera blocks.

track camera will control the mirror, and by using {0,0,1,0} the compensated track camera is selected. The sign inversion necessary for proper command of the mirror is inserted in the last summation block just before the output of the subsystem. This technique not only allows for the selection of one set of commands, but also allows for the combination of commands from multiple sources. For example, by using {0.5,0,0.5,0} the average between the uncompensated track camera and the compensated track camera can be used to command the steering mirror.

3.4 Summary

In this chapter, we have developed some relations to describe the turbulence levels in the experiment. We have also described the particular simulation technique that was utilized. We reviewed each segment of the simulation, how it works, and how the segments were set up to work together. We also noted that each random realization was 4 time steps long, allowing the delays from all of the sensors to the control elements to propagate through and bring the system to a steady state. The next chapter will look at the results from all of the simulations.

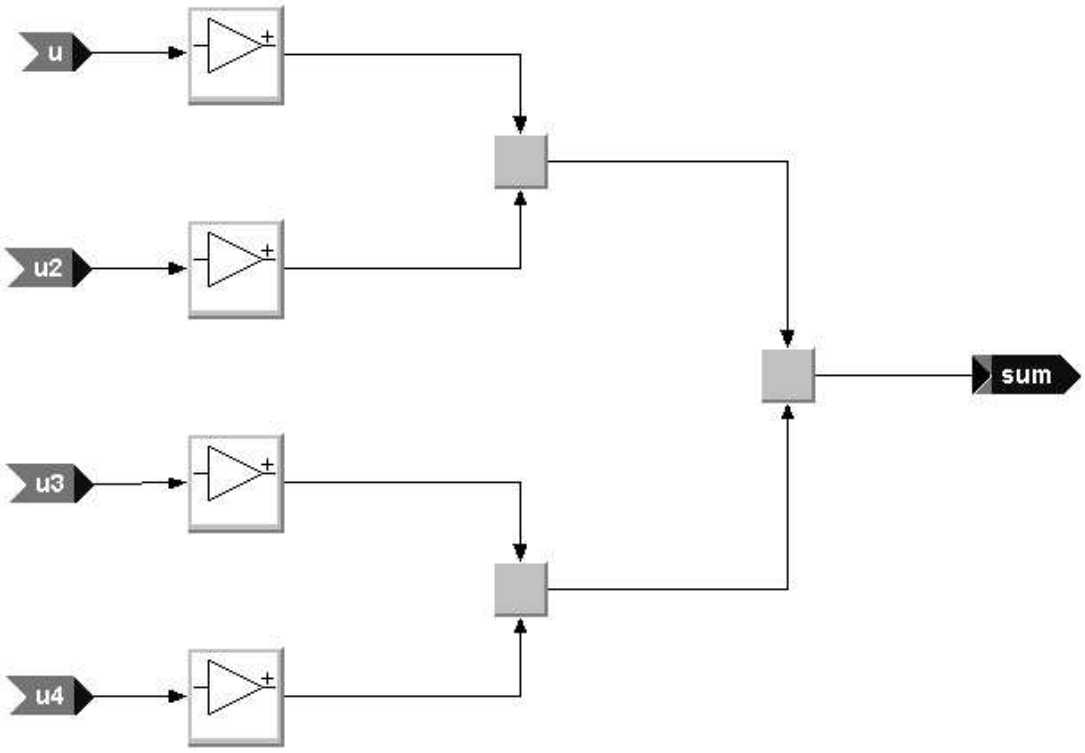

Figure 3.7. The control selector.

IV. Results

4.1 Introduction

This chapter examines the results of the propagation simulations that were conducted. It is divided into two main sections dealing with the point source experiments first and then the extended source experiments. The point source and extended source were done in the same manner using the same random seeds. Each set consisted of 80 random samples, 21 different separations between the track beacon and adaptive optics beacon, and 10 values of r_0 for compensated tracking. The complete list of system parameters are shown in Table 4.1. The uncompensated sets were identical save for the fact that only one separation was used, since the placement of the adaptive optics beacon was irrelevant to the uncompensated results.

Parameter	Value(s)	Units
r_0	{10,9,8,7,6,5,4,3,2,1}	cm
No. of Realizations	80	NA
Beacon Separations	{0,2.5,5,7.5,...,47.5,50}	cm
Range	50	km
No. of Phase Screens	5	NA
HEL Wavelength	1.000	μm
BILL Wavelength	0.999	μm
TILL Wavelength	1.001	μm
FSM Time Constants	1	μs
Target Board Resolution	1	cm
Target Board Size (H x W)	2.56 x 2.56	m
Propagation Grid Size	256 x 256	NA
Propagation Grid Spacing	1	cm
Camera IFOV	0.2	μrad
Camera Size	256 x 256	pixels
Platform Height	2400	m
Target Height	2400	m

Table 4.1. Parameters used for the simulation.

4.2 Turbulence Levels

As it turns out, the turbulence levels chosen for these simulation runs tend to be very strong. The method used for determining the turbulence level in WaveTrain under-represents the actual level of turbulence. The parameter r_0, developed originally for astronomical type viewing, takes into consideration primarily the near field turbulence. For a vertical path this is fine, but for horizontal paths it is not. Table 4.2 shows the chosen values of r_0 compared with other methods of measuring turbulence. In this table, along side r_0 and θ_0, the corresponding values for C_n^2, Rytov

r_0 (cm)	θ_0 (μrad)	C_n^2	Rytov Variance	Clear 1 Factor
10	0.63	$1.48x10^{-16}$	0.642	2.97
9	0.57	$1.77x10^{-16}$	0.765	3.54
8	0.50	$2.15x10^{-16}$	0.931	4.30
7	0.44	$2.69x10^{-16}$	1.16	5.38
6	0.38	$3.48x10^{-16}$	1.50	6.95
5	0.31	$4.71x10^{-16}$	2.04	9.42
4	0.25	$6.83x10^{-16}$	2.95	13.7
3	0.19	$1.10x10^{-15}$	4.77	22.1
2	0.13	$2.17x10^{-15}$	9.38	43.4
1	0.063	$6.89x10^{-15}$	29.8	138

Table 4.2. Other parameters for measuring turbulence level. Even at the weakest turbulence level used, the level of turbulence is very high.

variance, and Clear 1 Factor are shown. C_n^2 was derived using Equation (3.1). The Rytov variance [3] represents the irradiance fluctuations of the wave at the receiver. It is defined by the equation

$$\sigma_1^2 = 0.123 C_n^2 k^{7/6} L^{11/6} \tag{4.1}$$

Weak fluctuations are associated with $\sigma_1^2 \ll .1$ while strong fluctuation are associated with $\sigma_1^2 \gg .1$. Table 4.2 indicates that the turbulent levels chosen are clearly in the strong fluctuation region. The other parameter, Clear 1 Factor, is simply a scaling of C_n^2 by a value of $5x10^{-17}$. A Clear 1 Factor of 1 is the baseline design criterion for

the Airborne Laser. Table 4.2 shows that the turbulence levels chosen go far beyond the reasonable conditions that the Airborne Laser would experience. It would have been better to determine the turbulence strength by C_n^2 and Rytov variance, as well as r_0.

4.3 Point Source Results

The point source results follow. First some sample images are shown, and then the pointing performance data.

4.3.1 Test Images. Figures 4.1 through 4.3 show the uncompensated track beacon images at the observer. Each sub-figure is composed of four random samples at the same turbulence level. Across the sub-figures the same random seed is shown. This makes it appear like they are all pictures of the same object, just progressively blurrier. As can be seen in Figure 4.3, the cases in which r_0 is 2cm or less, the beacon begins to have portions outside the viewing area. For this reason the data at those extreme turbulence levels are omitted from the rest of the results. Also, even for the weaker turbulence levels, significant spot breakup can be noted. This speckling of the image causes bright and dark spots to appear, which could have a significant effect on the centroid, since it is an intensity weighted measurement. This speckling would also affect the performance of the adaptive optics compensation. Figures 4.4 and 4.5 show the compensated images of the track beacon.

Figures 4.6 and 4.7 show the scoring beam as seen by the target board. These are shown in the same way as in Figures 4.1 through 4.3, with four random samples per sub-figure. The overall impression is the same, with the ultimate result being that data at $r_0 = 2cm$ and $r_0 = 1cm$ is not able to be captured accurately.

4.3.2 Tilt Performance. Tracking performance is often measured in terms of jitter, or tilt variance. Figures 4.8 and 4.9 show resulting error variance at the target board for both compensated and uncompensated tracking. The graphs show

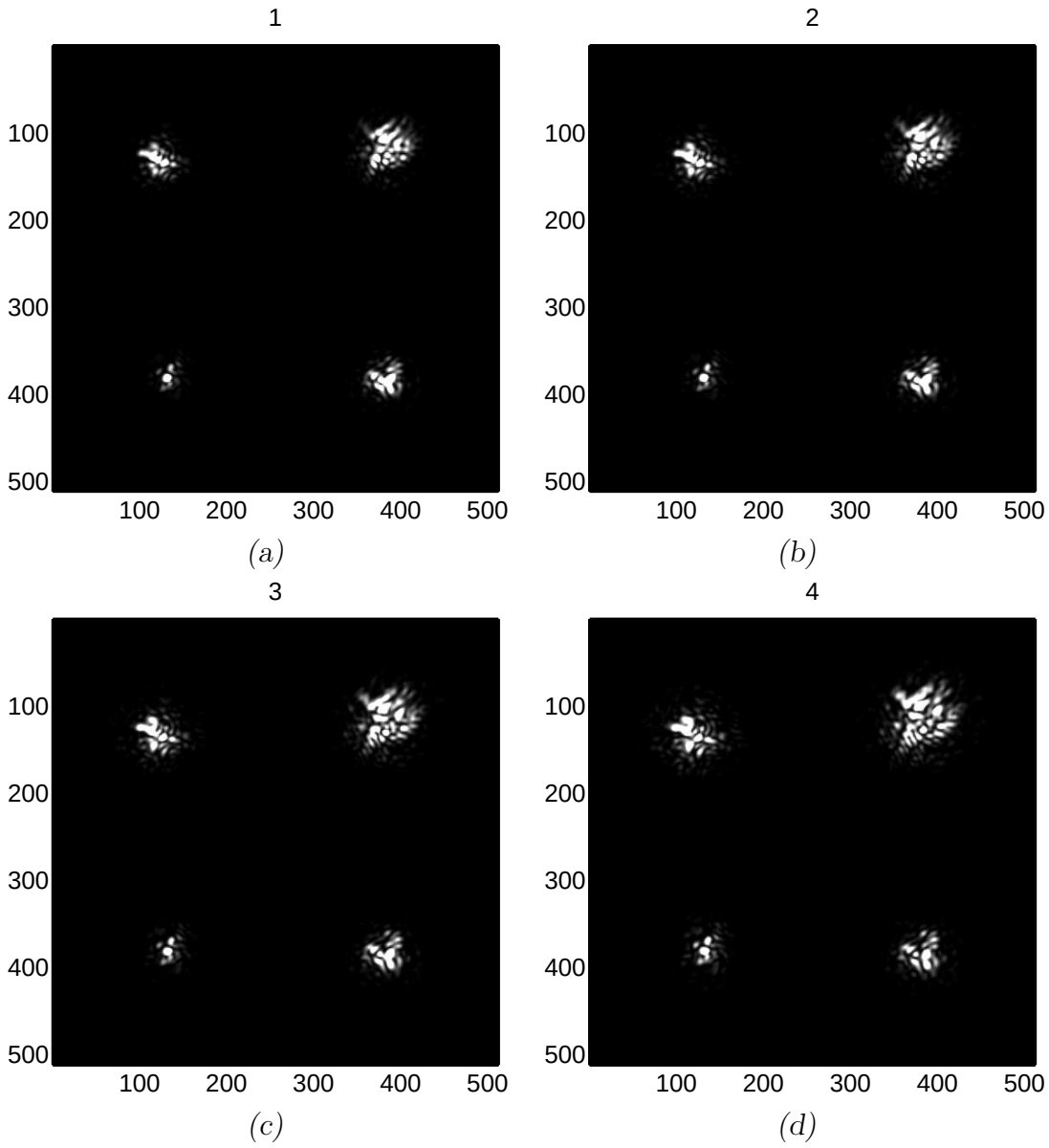

Figure 4.1. *Sample images of the point source track beacon. Each sub-figure shows four different realizations. (a) $r_0 = 10cm$ (b) $r_0 = 9cm$ (c) $r_0 = 8cm$ (d) $r_0 = 7cm$*

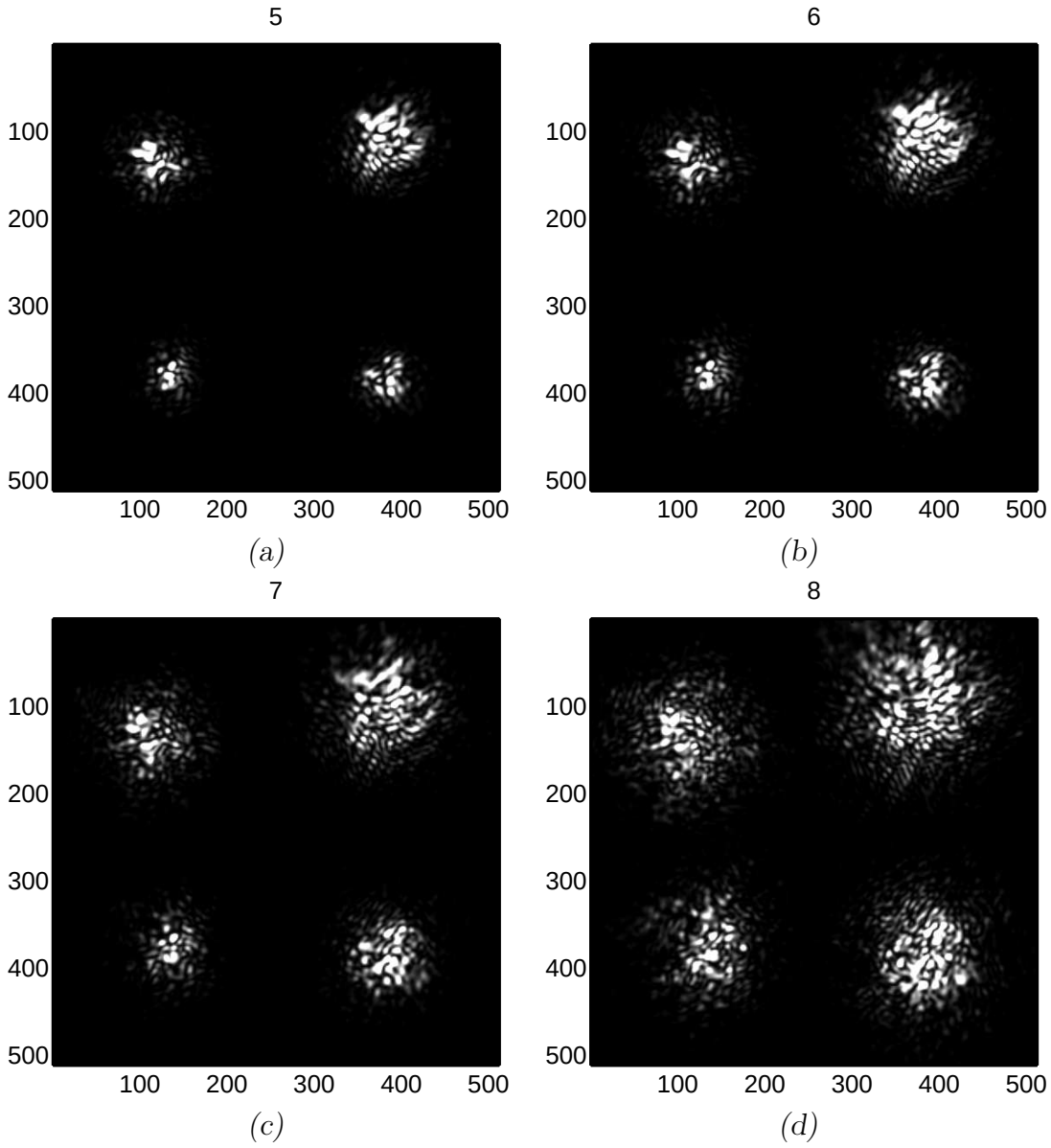

Figure 4.2. *More sample images of the point source track beacon. (a) $r_0 = 6cm$ (b) $r_0 = 5cm$ (c) $r_0 = 4cm$ (d) $r_0 = 3cm$*

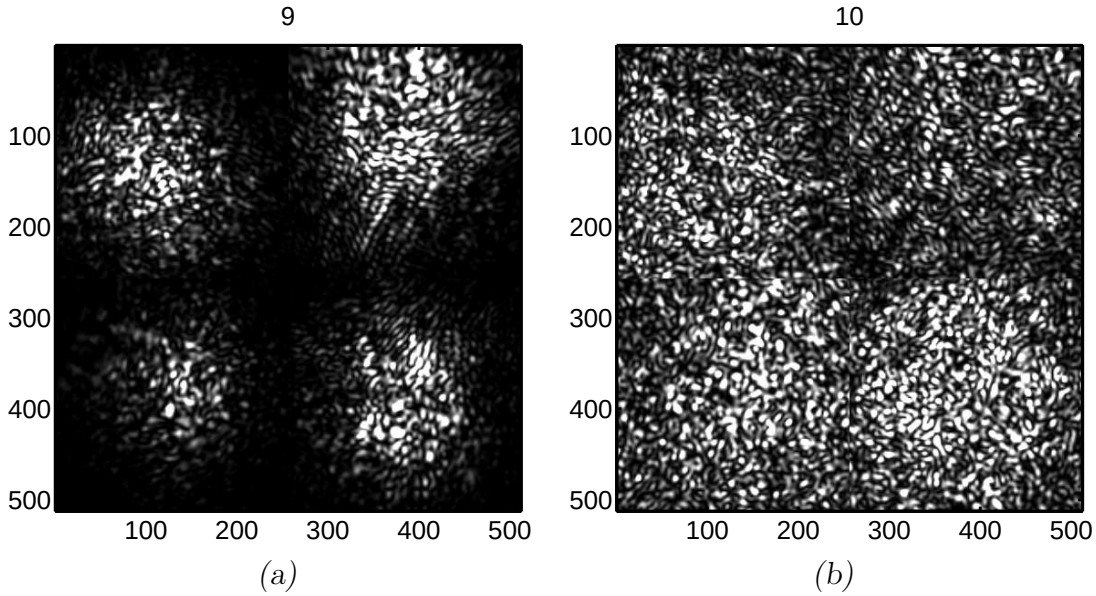

Figure 4.3. *Sample images of the point source track beacon. (a) $r_0 = 2cm$ (b) $r_0 = 1cm$*

variance as a function of separation between the adaptive optics beacon and the target beacon. As expected, the tracking performance increases (tilt variance is reduced) when the higher order compensator is used. There are a couple of notable abnormalities in the results for tilt variance. These occur on Figure 4.8 (a) and (c). These spikes, in each of the three cases, result from a single run producing an abnormally high tilt error (the difference between the center of the target board and the measured centroid). It appears that in each case the steering mirror had not settled, causing the large error. The steering mirrors all have time constants of 1μs, meaning each would reach a steady state value before the next time step. However, in each of these anomalies the tilt error is exactly the same for the third and fourth time step (remembering that each run is four time steps long). This would indicate that the steering mirror did not receive the command to move before the fourth time step. All attempts to recreate these anomalies failed.

Figures 4.10 through 4.13 show the tilt error for first the x axis and then the y axis. Keep in mind the adaptive optics beacon was moved along the x axis. The

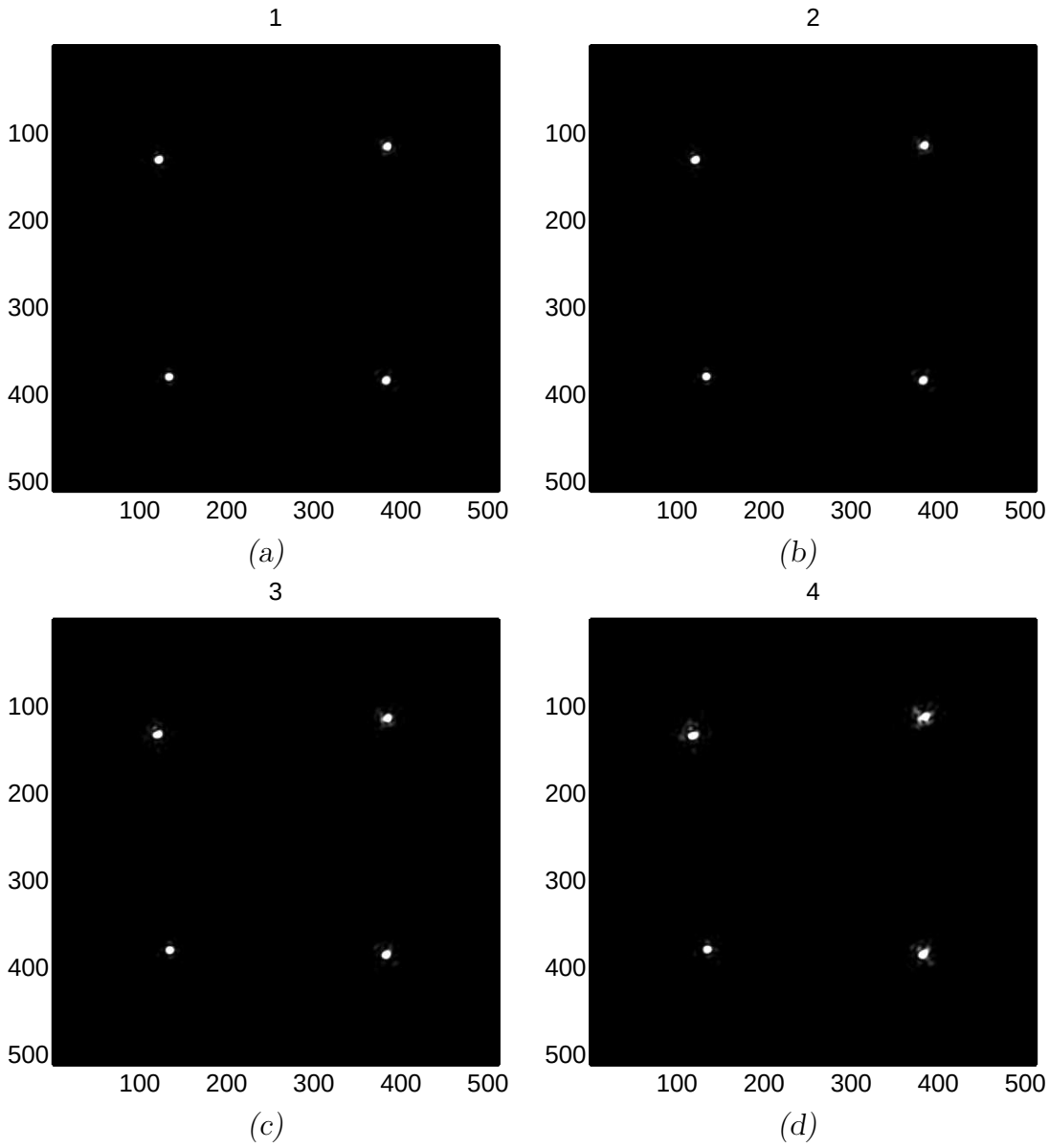

Figure 4.4. *Sample images of the compensated point source track beacon. Note that the adaptive optics system degradation as the turbulence level increased (a) $r_0 = 10cm$ (b) $r_0 = 9cm$ (c) $r_0 = 8cm$ (d) $r_0 = 7cm$*

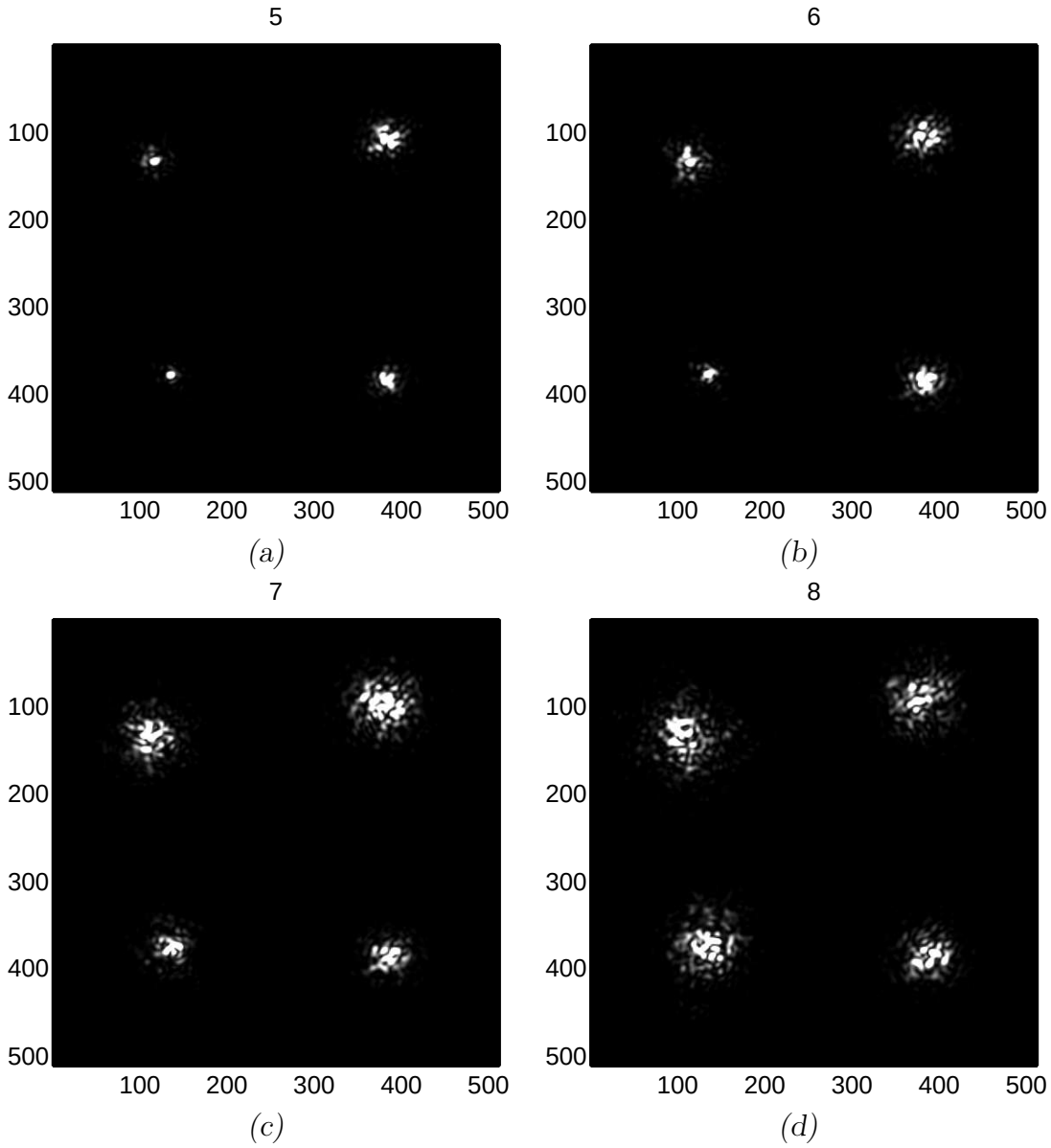

Figure 4.5. *More sample images of the compensated point source track beacon. (a) $r_0 = 6cm$ (b) $r_0 = 5cm$ (c) $r_0 = 4cm$ (d) $r_0 = 3cm$*

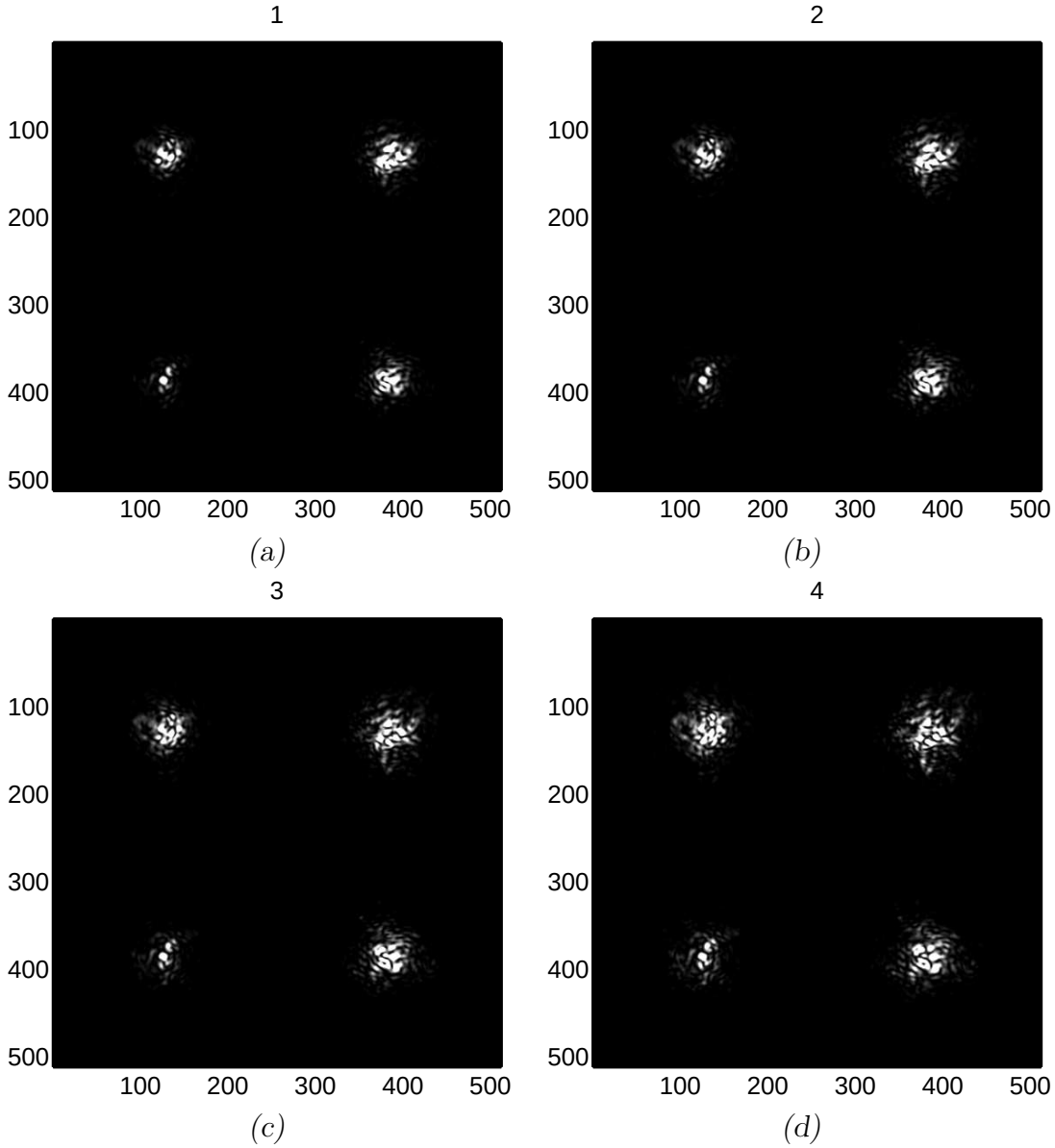

Figure 4.6. *Sample images at the target board. (a) $r_0 = 10cm$ (b) $r_0 = 9cm$ (c) $r_0 = 8cm$ (d) $r_0 = 7cm$*

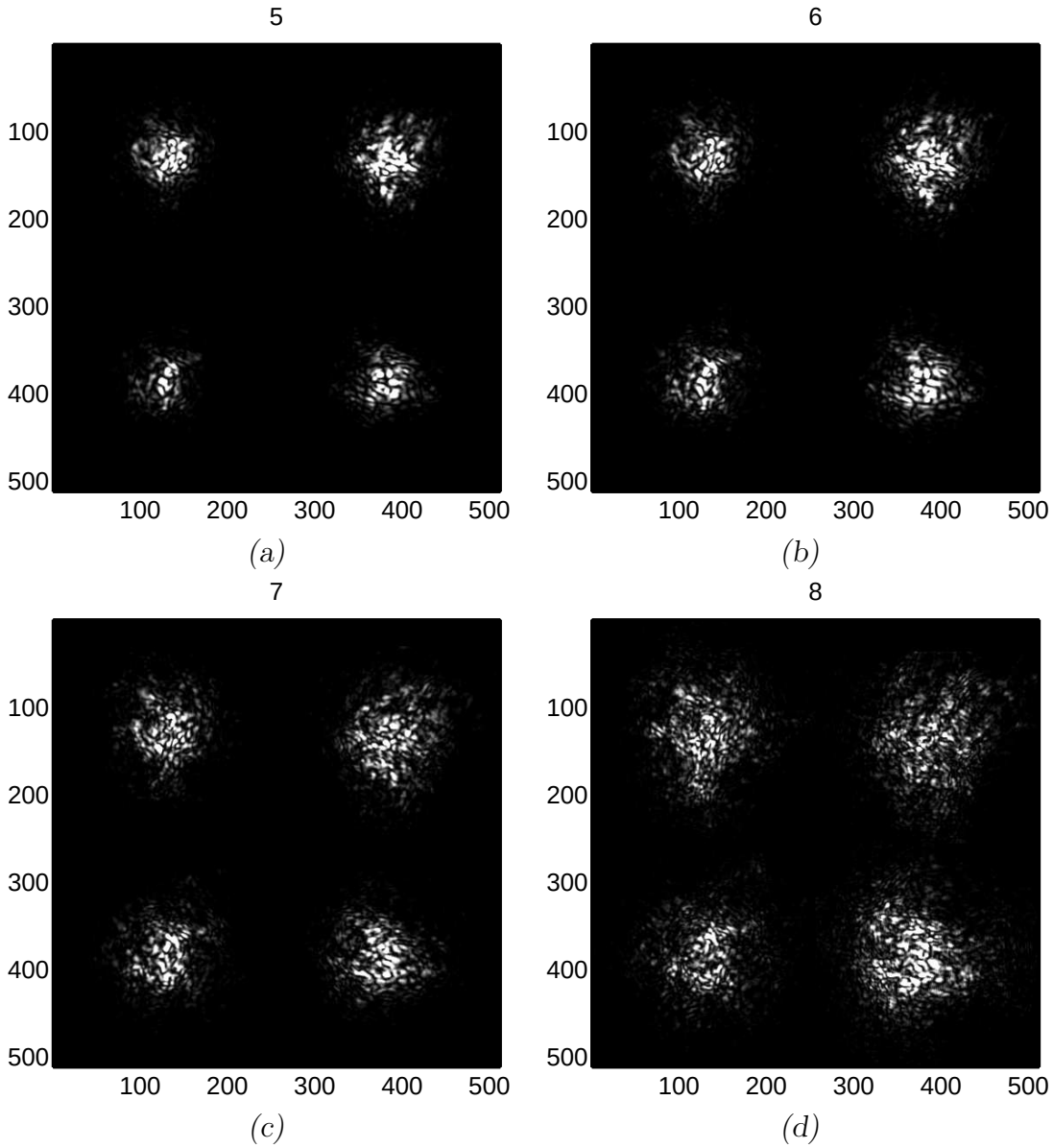

Figure 4.7. *Sample images at the target board. (a) $r_0 = 6cm$ (b) $r_0 = 5cm$ (c) $r_0 = 4cm$ (d) $r_0 = 3cm$*

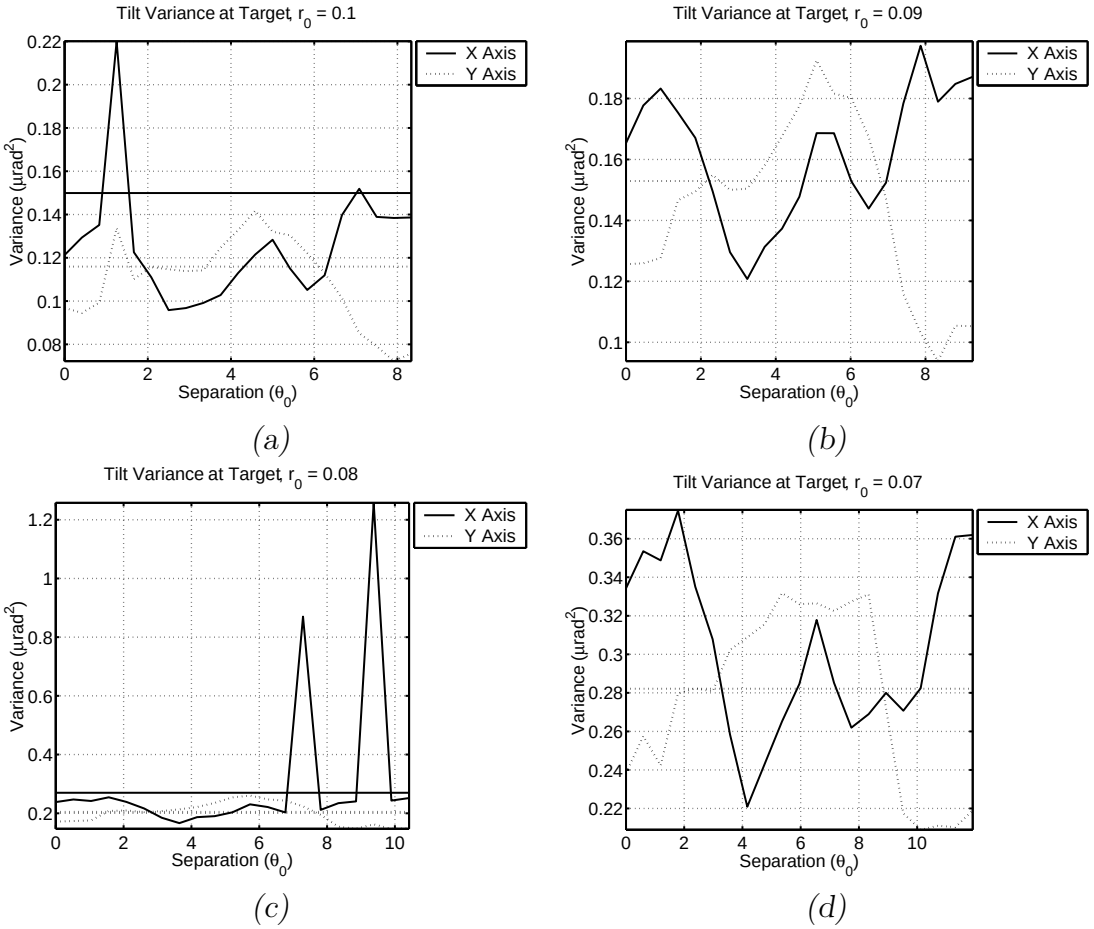

Figure 4.8. *Tilt variance. Each sub-figure shows the tilt variance for compensated and uncompensated (a horizontal line since it is independent of beacon separation) as a function of separation between the adaptive optics beacon and the track beacon. Beacon separation is measured in values of θ_0. The spikes in (a) and (c) are the results of a single run in each case. These anomalies were likely the results of the steering mirror not reaching its final state properly. Attempts to reproduce the specific error failed. (a) $r_0 = 10cm$ (b) $r_0 = 9cm$ (c) $r_0 = 8cm$ (d) $r_0 = 7cm$*

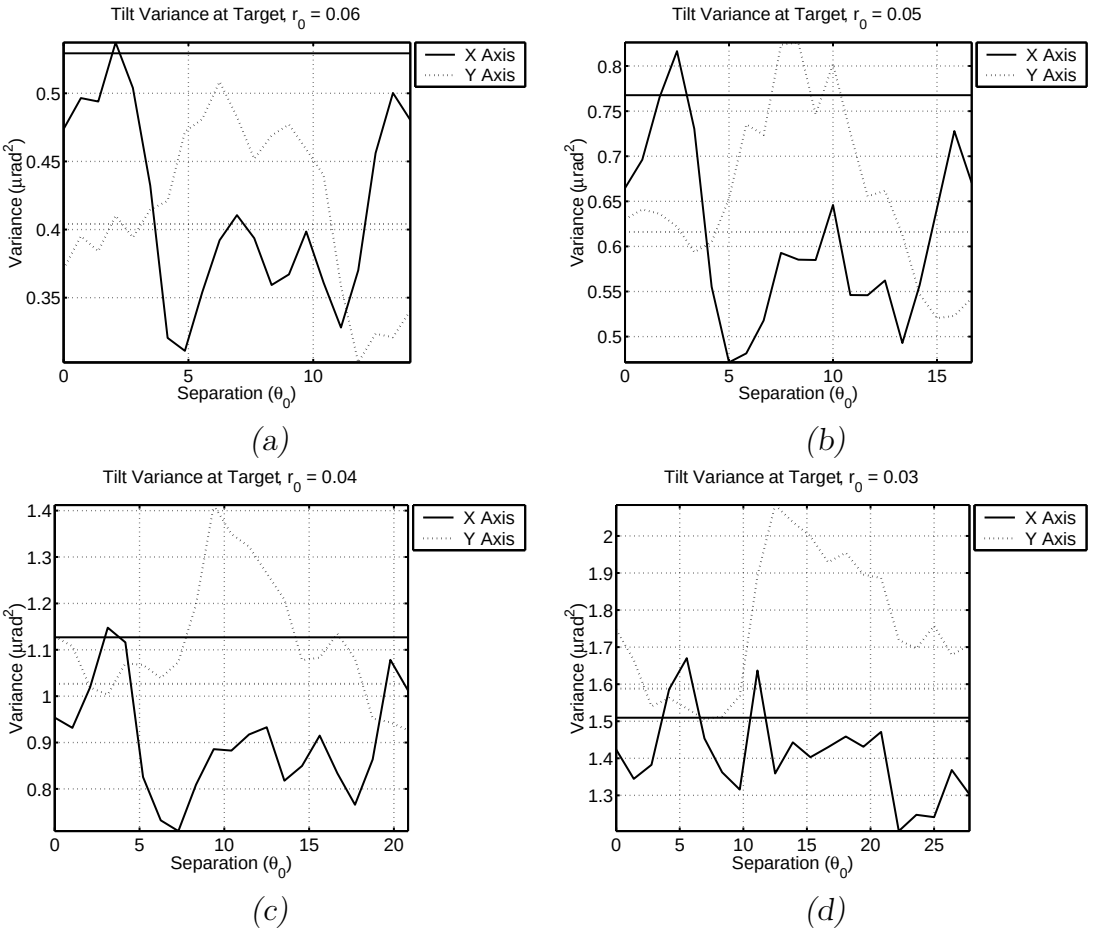

Figure 4.9. *Tilt variance. Each sub-figure shows the tilt variance for compensated and uncompensated (a horizontal line since it is independent of beacon separation) as a function of separation between the adaptive optics beacon and the track beacon. Beacon separation is measured in values of* θ_0*. (a)* $r_0 = 6cm$ *(b)* $r_0 = 5cm$ *(c)* $r_0 = 4cm$ *(d)* $r_0 = 3cm$

dominant feature in the x axis is the tendency to move towards the positive as the beacon moves more negative. The likely explanation is an overcorrection of tilt by the tilt-removal section of the compensator block. This is probably a result of part of the return from the beacon being moved off the detector. This would then result in an under-representation of the actual tilt, therefore causing the error. The other notable effect is the apparent bias in the y axis that appears as the beacon is moved. It seems that the effect is a result of the anisoplanatic compensation and not from an artifact of the simulation. However, if the anisoplanatic compensation were having an effect on the ability of the system to track the target, then the variance would have increased as well.

4.4 Extended Source Results

The extended source results follow. First some track beacon and target board image samples are shown, and then the pointing performance data.

4.4.1 Test Images. Figures 4.14 and 4.15 show the uncompensated track beacon images at the observer. Each sub-figure is actually composed of four random samples at the same turbulence level. Across the sub-figures the same random seed is shown. This makes it appear like they are all pictures of the same object, just progressively blurrier. It is also interesting to observe the track beacon using compensated images, shown in Figures 4.16 and 4.17. The shape of the 32cm by 16cm rectangle target can be clearly seen in the lower turbulence cases.

4.4.2 Tilt Performance. Figures 4.18 and 4.19 show resulting error variance at the target board for both compensated and uncompensated tracking. Figures 4.20 through 4.23 show the tilt error for first the x axis and then the y axis.

The results for the extended source are very similar to that of the point source. This is likely due to the method of tracking and the nature of the target. In both cases a centroid tracker was used to track a symmetrical target. Without the tracker being

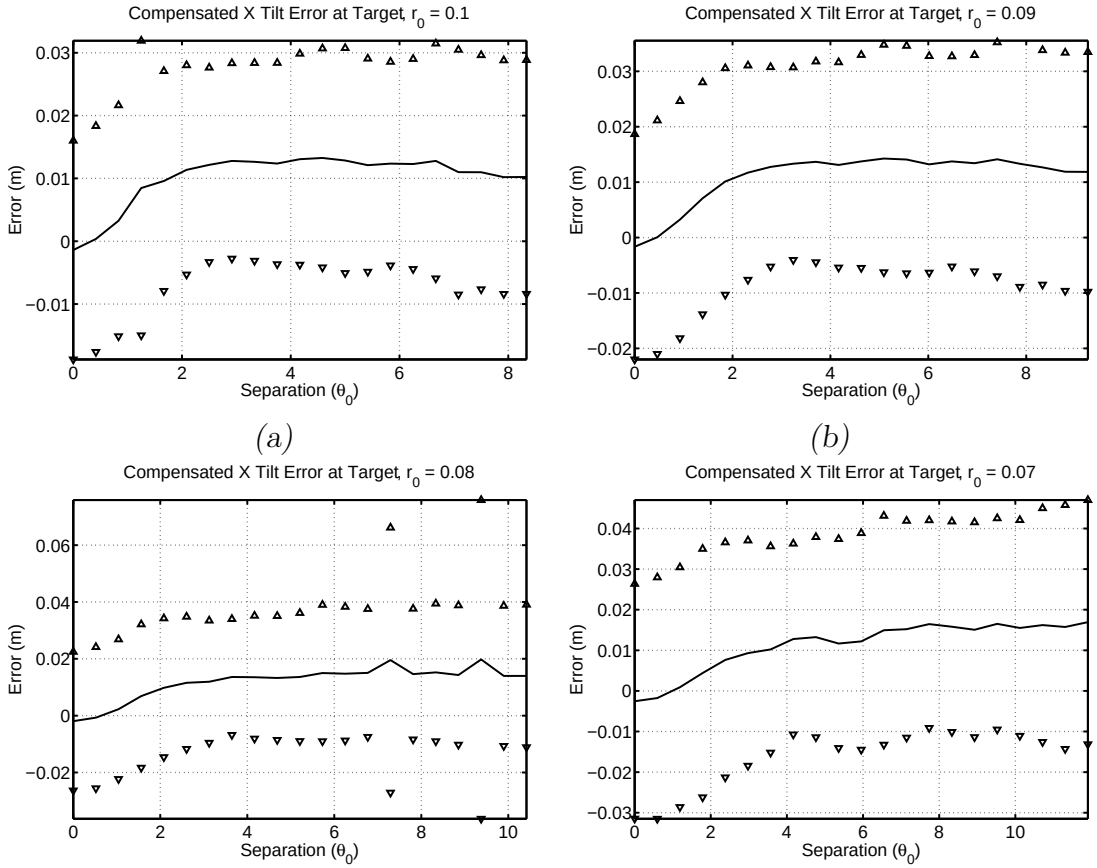

Figure 4.10. *X Tilt error. Each sub-figure shows the tilt error for compensated and uncompensated (a horizontal line since it is independent of beacon separation) as a function of separation between the adaptive optics beacon and the track beacon. Beacon separation is measured in values of* θ_0*. (a)* $r_0 = 10cm$ *(b)* $r_0 = 9cm$ *(c)* $r_0 = 8cm$ *(d)* $r_0 = 7cm$

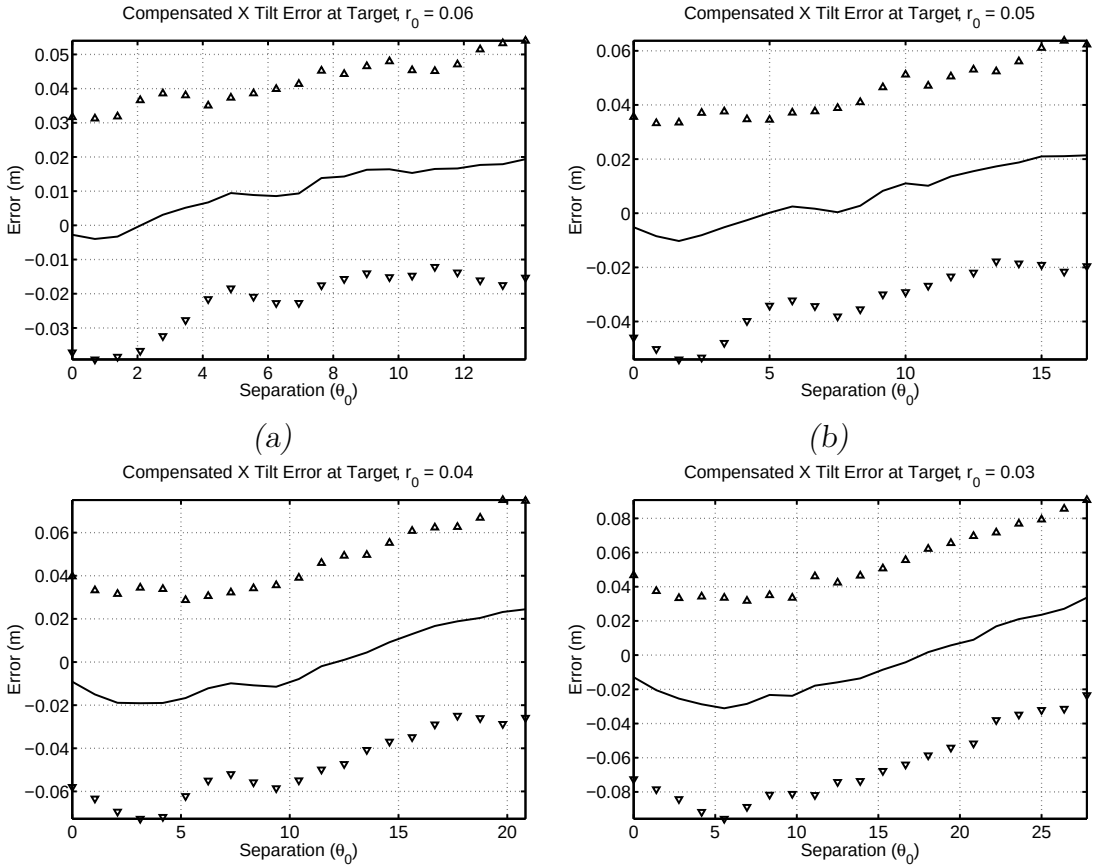

Figure 4.11. *Tilt error. Each sub-figure shows the tilt error for compensated and uncompensated (a horizontal line since it is independent of beacon separation) as a function of separation between the adaptive optics beacon and the track beacon. Beacon separation is measured in values of* θ_0. *(a)* $r_0 = 6cm$ *(b)* $r_0 = 5cm$ *(c)* $r_0 = 4cm$ *(d)* $r_0 = 3cm$

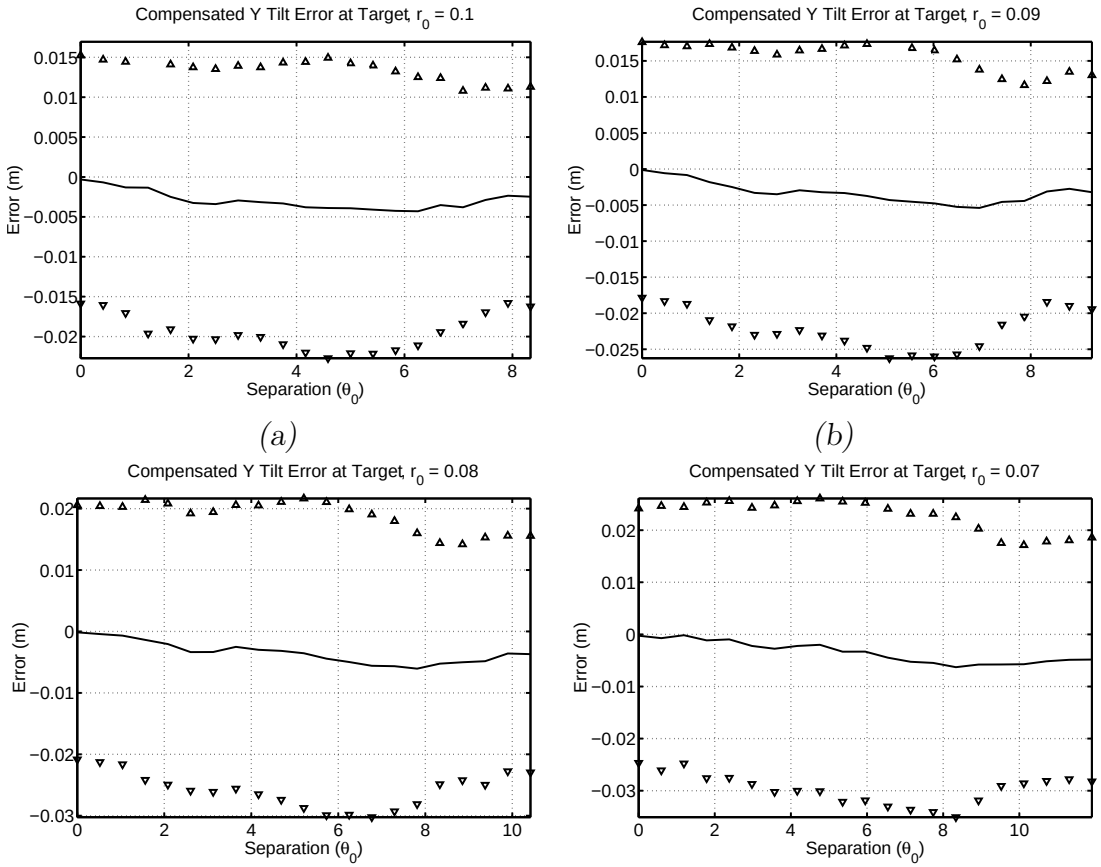

Figure 4.12. *Y Tilt error. Each sub-figure shows the tilt error for compensated and uncompensated (a horizontal line since it is independent of beacon separation) as a function of separation between the adaptive optics beacon and the track beacon. Beacon separation is measured in values of* θ_0*. (a)* $r_0 = 10cm$ *(b)* $r_0 = 9cm$ *(c)* $r_0 = 8cm$ *(d)* $r_0 = 7cm$

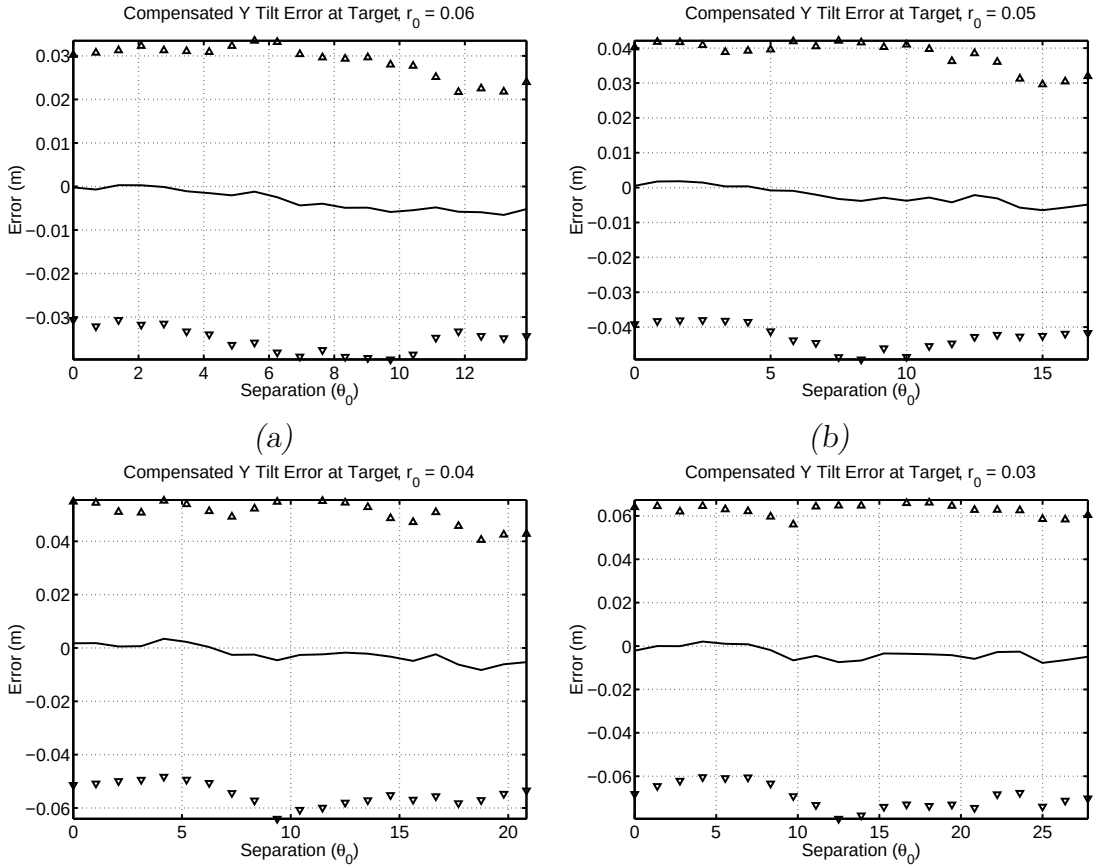

Figure 4.13. *Y Tilt error. Each sub-figure shows the tilt error for compensated and uncompensated (a horizontal line since it is independent of beacon separation) as a function of separation between the adaptive optics beacon and the track beacon. Beacon separation is measured in values of* θ_0*. (a)* $r_0 = 6cm$ *(b)* $r_0 = 5cm$ *(c)* $r_0 = 4cm$ *(d)* $r_0 = 3cm$

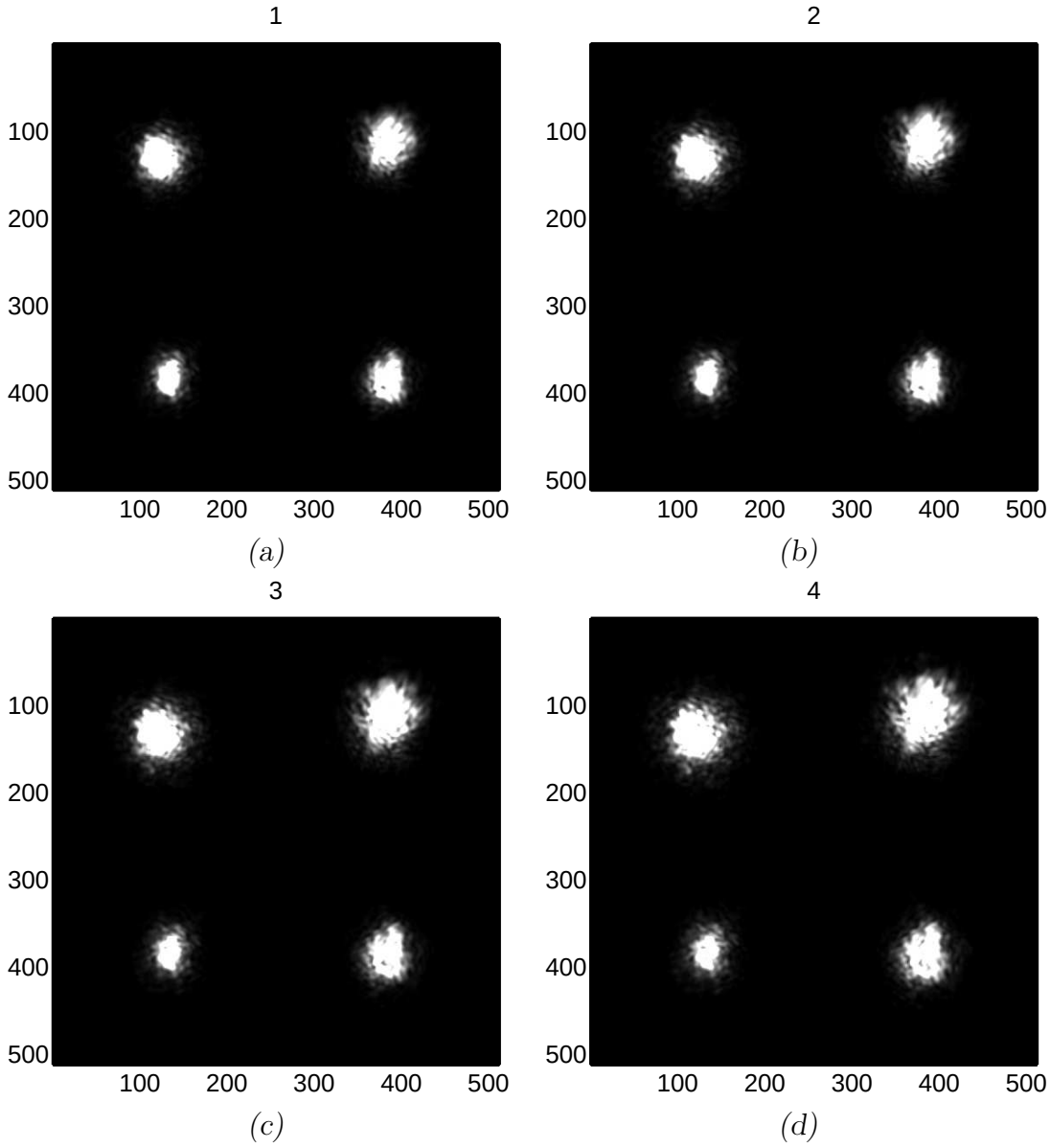

Figure 4.14. *Sample images of the uncompensated extended source track beacon. Each sub-figure shows four different realizations. (a) $r_0 = 10cm$ (b) $r_0 = 9cm$ (c) $r_0 = 8cm$ (d) $r_0 = 7cm$*

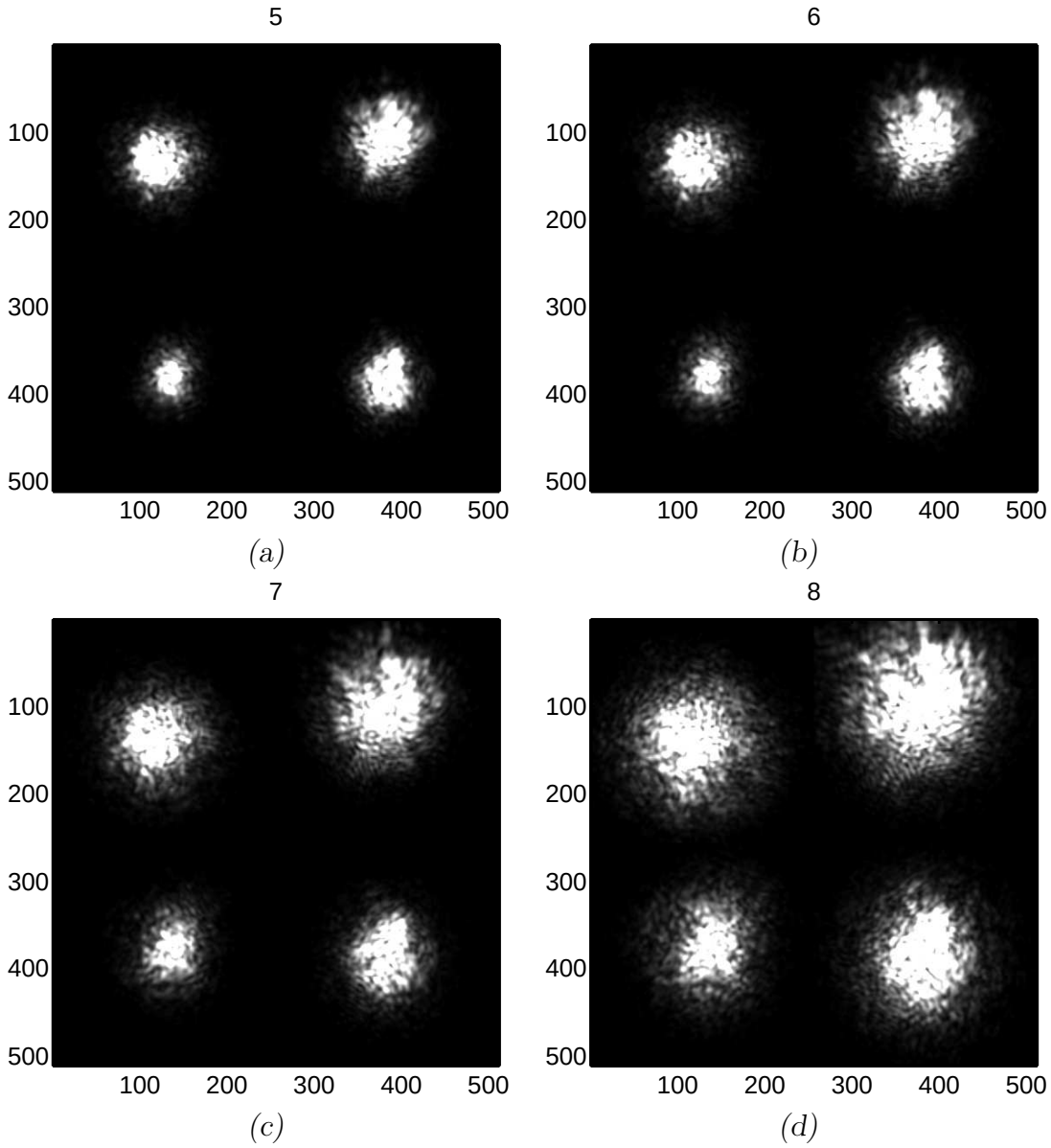

Figure 4.15. *Sample images of the uncompensated extended source track beacon. (a) $r_0 = 6cm$ (b) $r_0 = 5cm$ (c) $r_0 = 4cm$ (d) $r_0 = 3cm$*

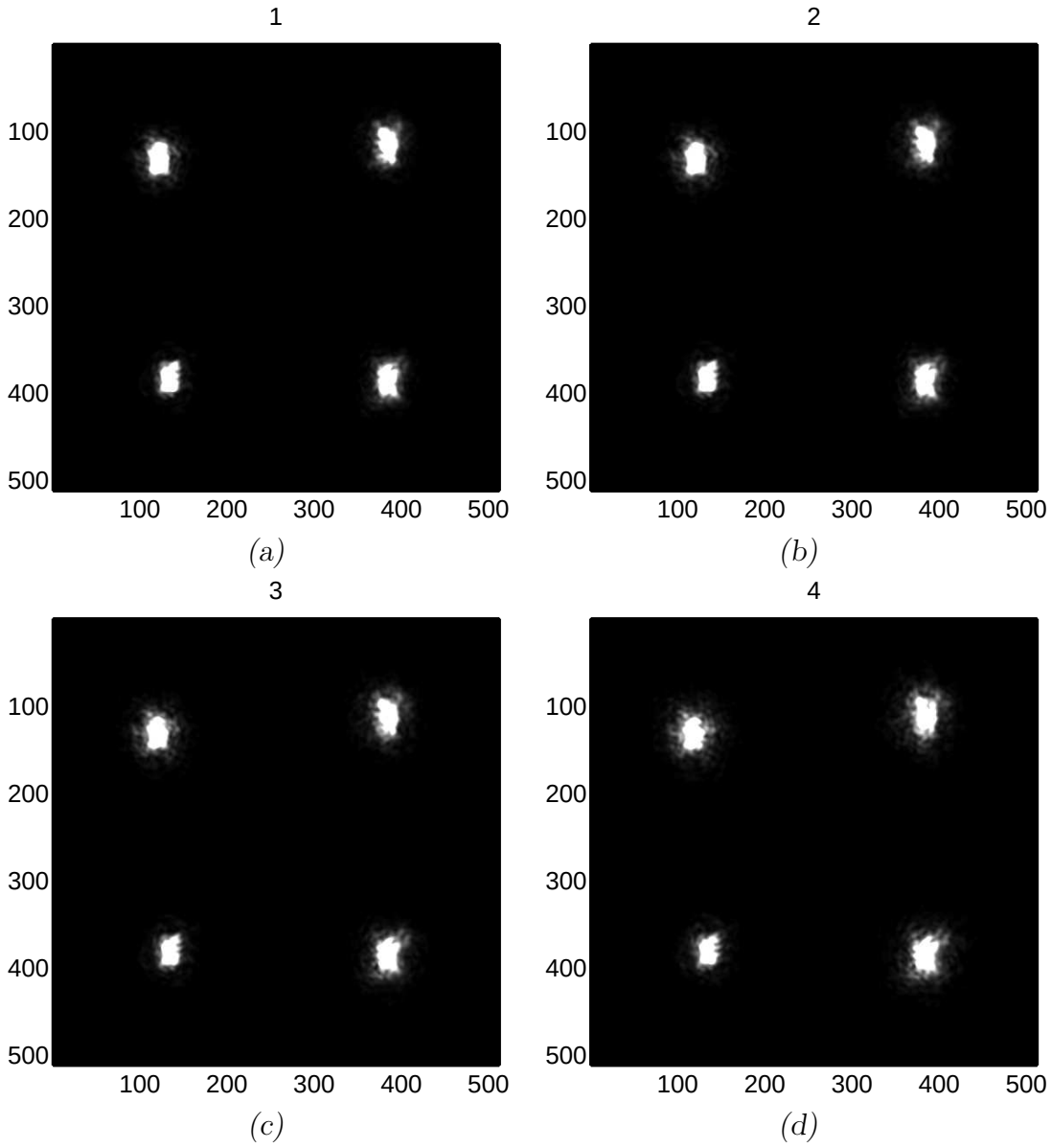

Figure 4.16. *Sample images of the compensated extended source track beacon. (a) $r_0 = 10cm$ (b) $r_0 = 9cm$ (c) $r_0 = 8cm$ (d) $r_0 = 7cm$*

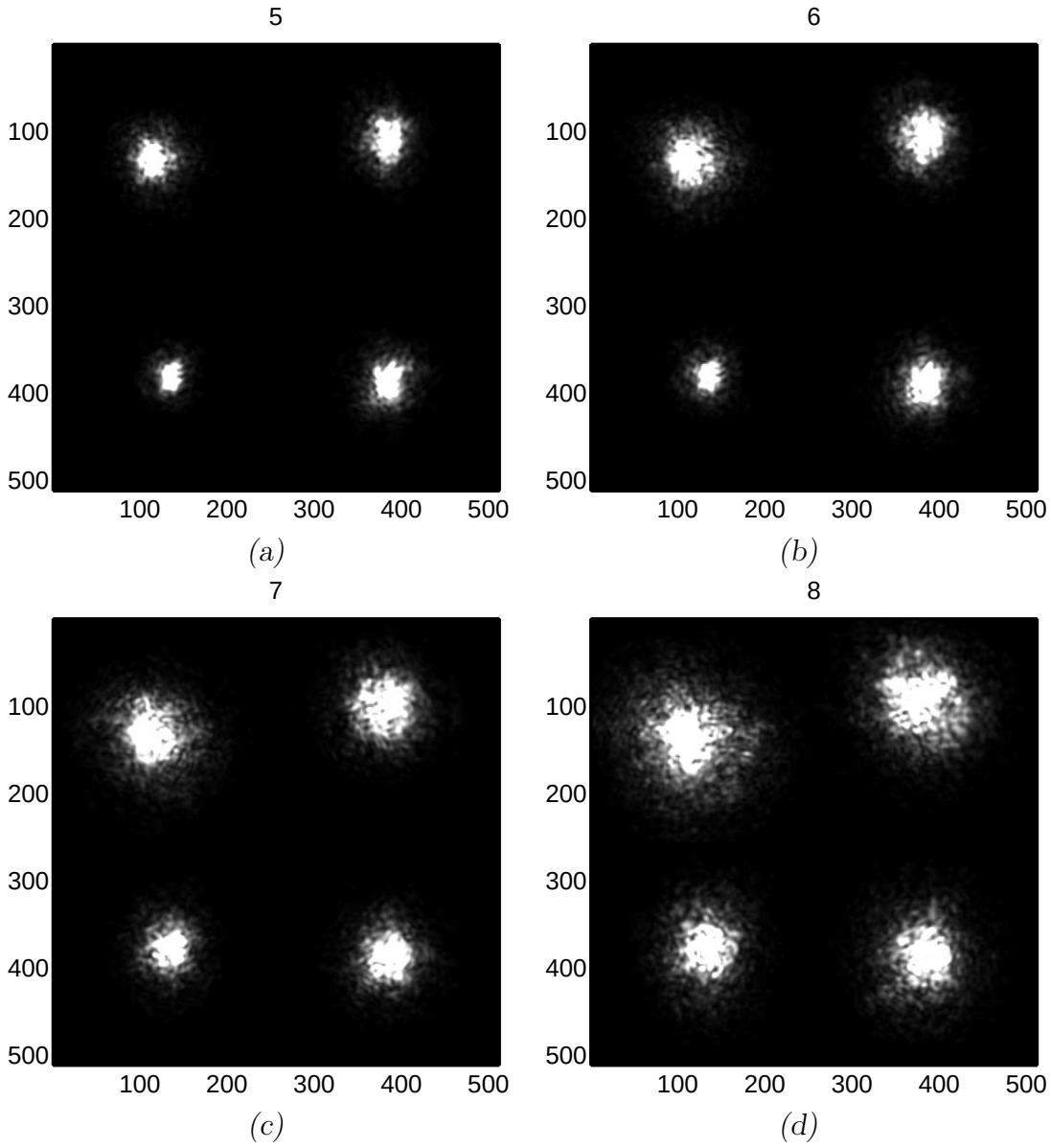

Figure 4.17. *Sample images of the compensated extended source track beacon. (a) $r_0 = 6cm$ (b) $r_0 = 5cm$ (c) $r_0 = 4cm$ (d) $r_0 = 3cm$*

dependent on any particular features of the target, the adaptive optics compensation would have little effect on the tilt. Also, the movement of the x tilt error and y tilt error as a result of the beacon movement was very similar to that of the point source results. The x tilt error tended to move away from the adaptive optics beacon in the same fashion in the point source results. This could be primarily a result of the method of tilt removal before the adaptive optics compensation. The results for the y tilt error indicate the same sort of bias as in the point source results as the adaptive optics beacon is moved. This does not necessarily indicate a degradation in tracking performance (if it did the tilt variance would have increased also) but does indicate the movement of the adaptive optics beacon has an effect on the mean placement of the scoring beam on the target board. There is nothing in the simulation setup itself that moves in the y axis, therefore the bias must be a result of the movement of the beacon.

4.5 Summary

This chapter looked at the results from the simulation. The most notable feature is the slope of the tilt error. The error for the X axis tends to the positive as the separation increases. The adaptive optics beacon however is actually moved in the negative direction. The Y axis, on the other hand, does not appear to be affected by the displacement of the adaptive optics beacon at all. This indicates that the trend for the X axis likely had more to do with the system setup than the anisoplanatic compensation, otherwise the Y axis would have been affected in the same way.

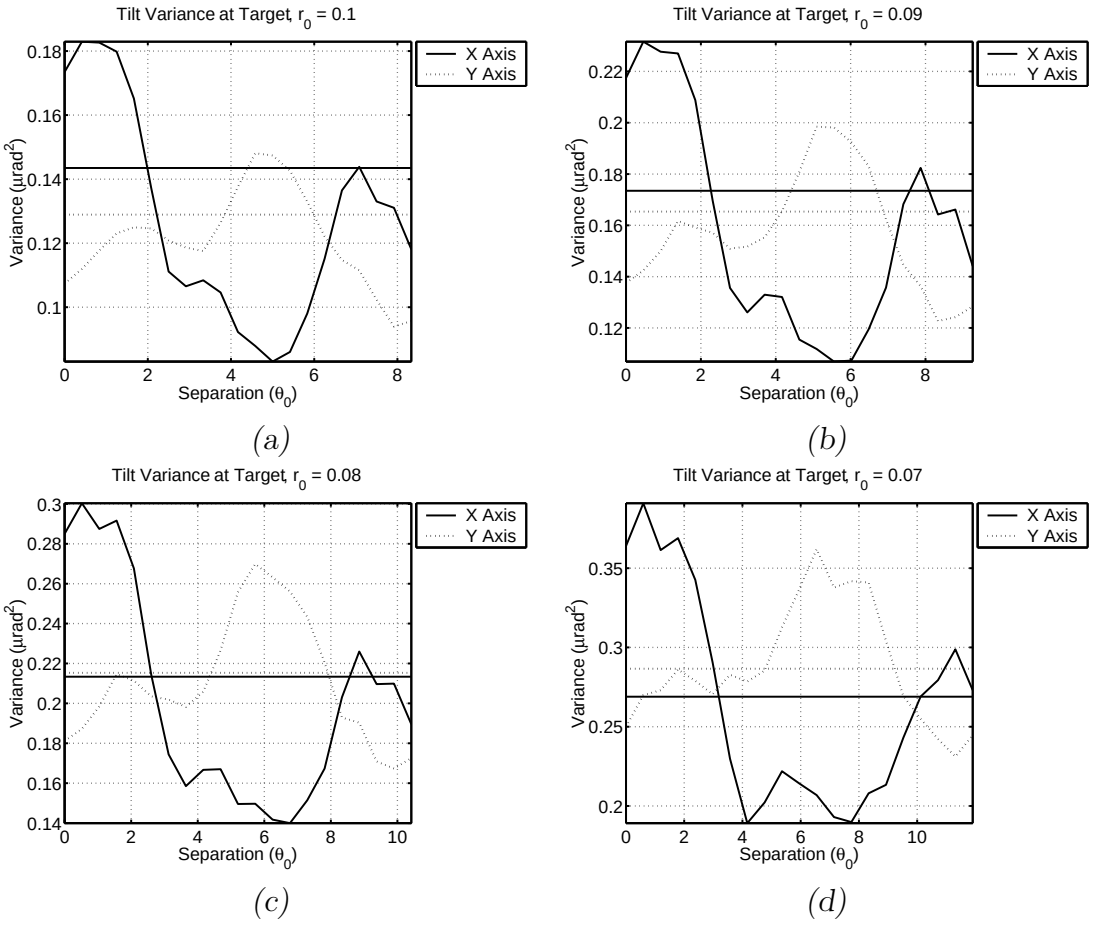

Figure 4.18. *Tilt variance. Each sub-figure shows the tilt variance for compensated and uncompensated (a horizontal line since it is independent of beacon separation) as a function of separation between the adaptive optics beacon and the track beacon. Beacon separation is measured in values of* θ_0. *(a)* $r_0 = 10cm$ *(b)* $r_0 = 9cm$ *(c)* $r_0 = 8cm$ *(d)* $r_0 = 7cm$

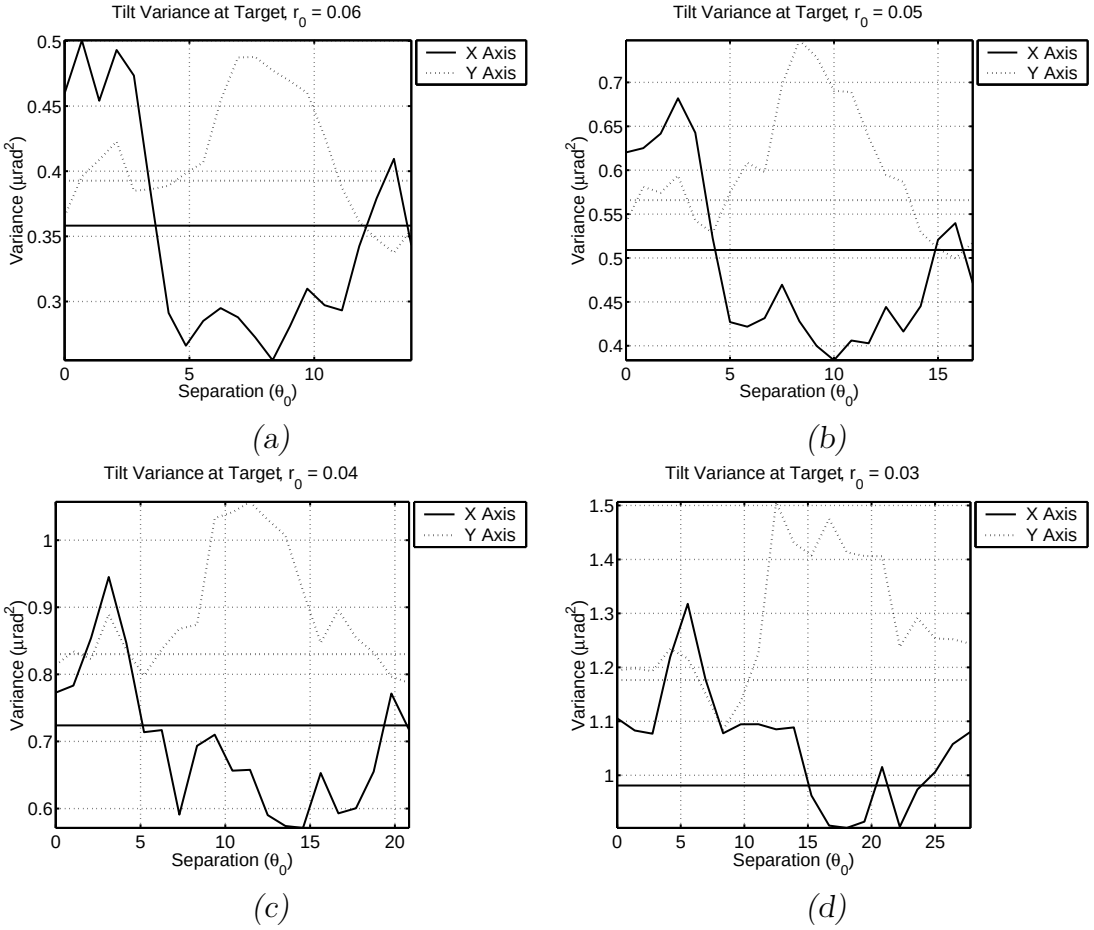

Figure 4.19. *More Tilt variance. (a) $r_0 = 6cm$ (b) $r_0 = 5cm$ (c) $r_0 = 4cm$ (d) $r_0 = 3cm$*

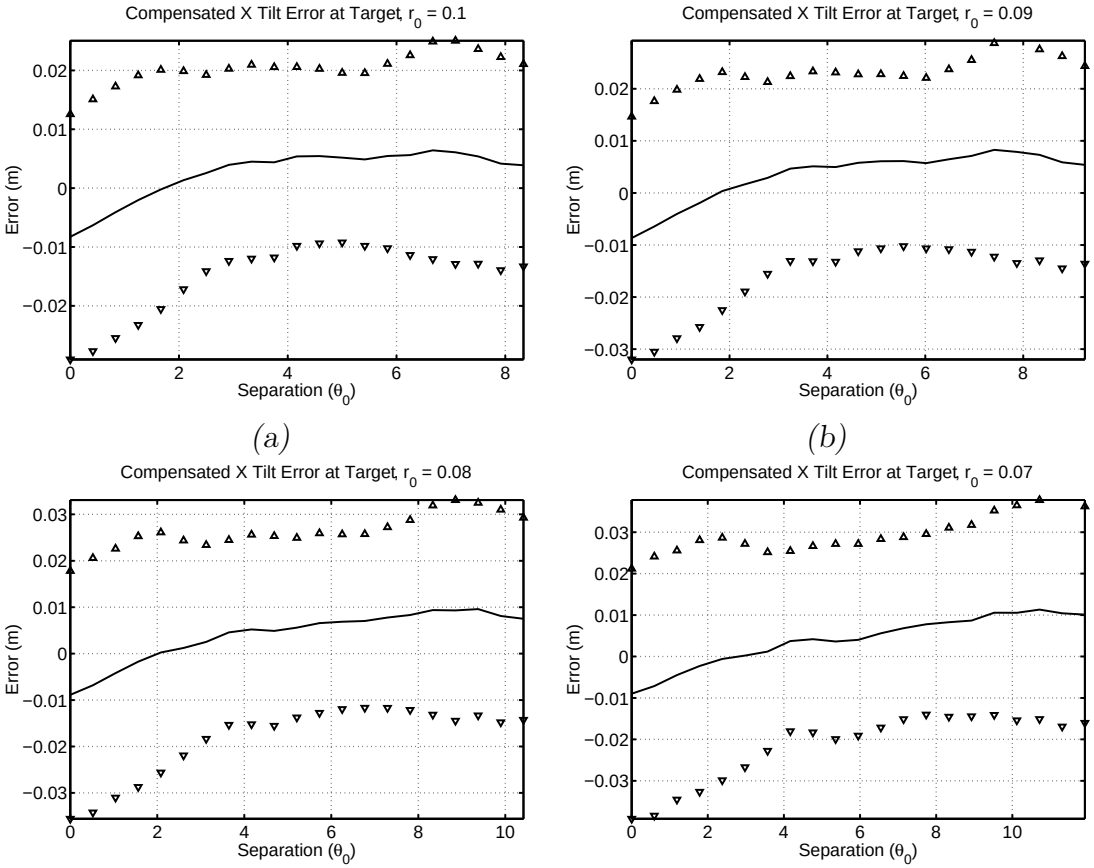

Figure 4.20. *X Tilt error. Each sub-figure shows the tilt error for compensated and uncompensated (a horizontal line since it is independent of beacon separation) as a function of separation between the adaptive optics beacon and the track beacon. Beacon separation is measured in values of* θ_0. *(a)* $r_0 = 10cm$ *(b)* $r_0 = 9cm$ *(c)* $r_0 = 8cm$ *(d)* $r_0 = 7cm$

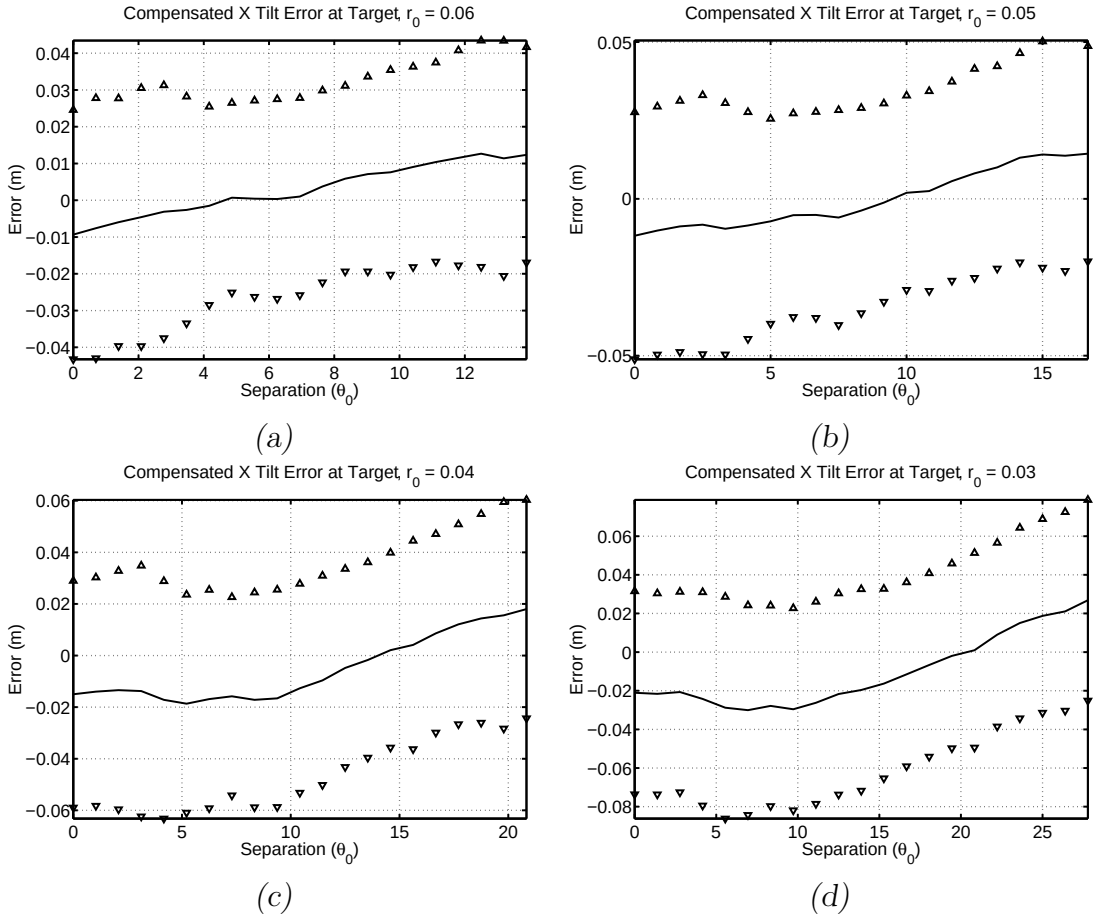

Figure 4.21. *More X Tilt error. (a) $r_0 = 6cm$ (b) $r_0 = 5cm$ (c) $r_0 = 4cm$ (d) $r_0 = 3cm$*

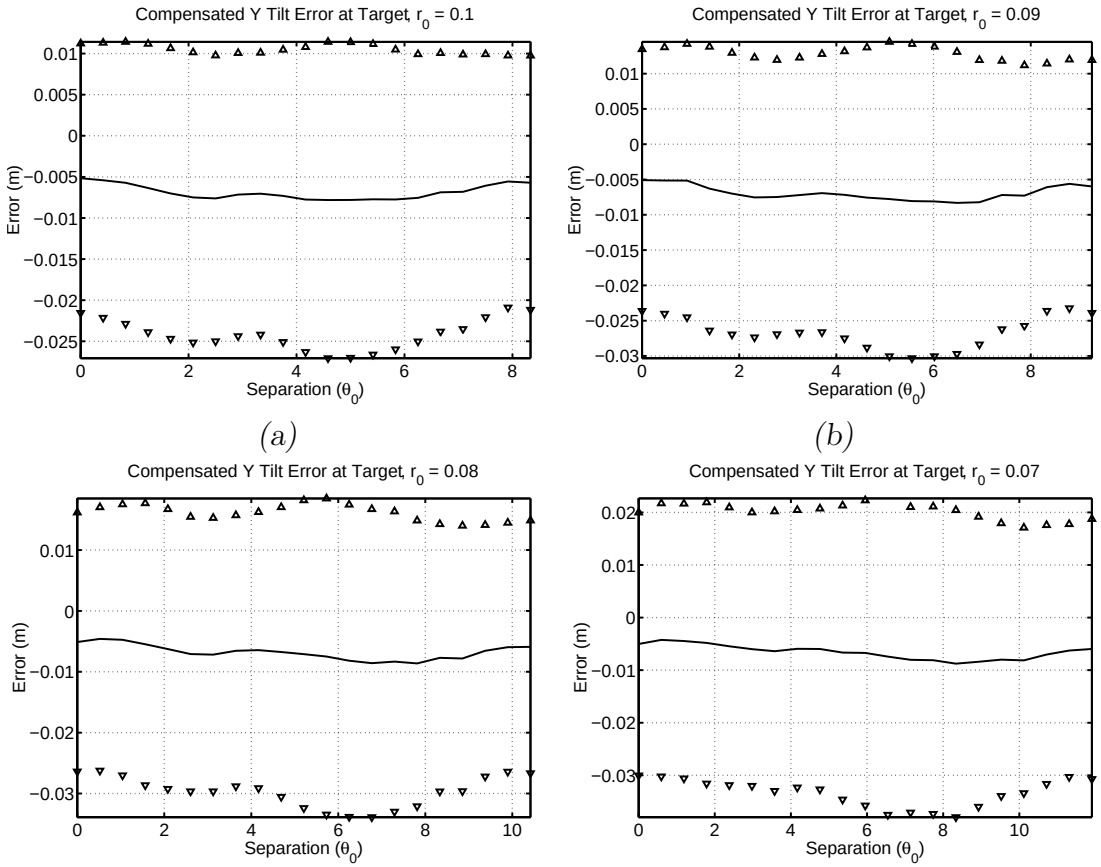

Figure 4.22. *Y Tilt error. Each sub-figure shows the tilt error for compensated and uncompensated (a horizontal line since it is independent of beacon separation) as a function of separation between the adaptive optics beacon and the track beacon. Beacon separation is measured in values of* θ_0*. (a)* $r_0 = 10cm$ *(b)* $r_0 = 9cm$ *(c)* $r_0 = 8cm$ *(d)* $r_0 = 7cm$

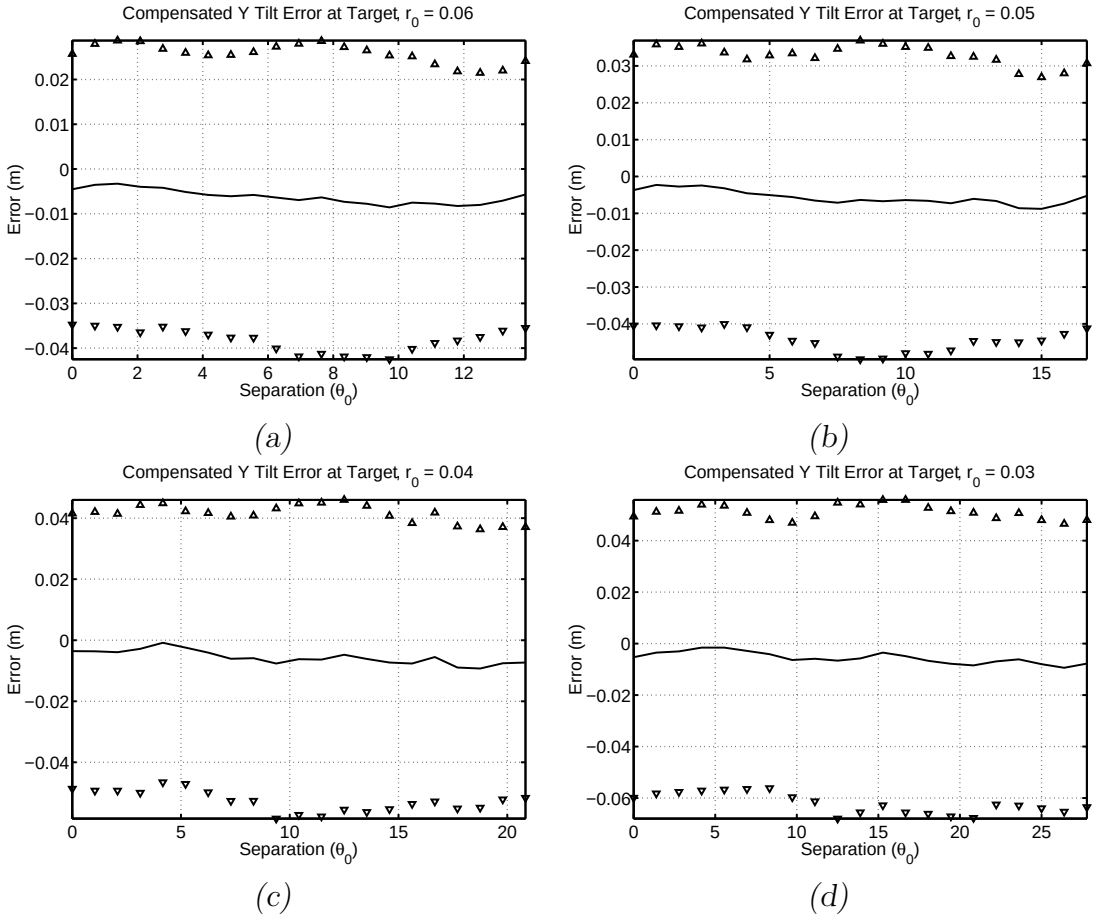

Figure 4.23. *More Y Tilt error. (a) $r_0 = 6cm$ (b) $r_0 = 5cm$ (c) $r_0 = 4cm$ (d) $r_0 = 3cm$*

V. Discussion and Future Work

5.1 Discussion

There are a couple of interesting ideas to come from this thesis. First, the development of a technique to measure the effect of anisoplanatic compensation on tracking was developed. This method allows for the further analysis of other types of scenarios to be explored. Second, and most importantly, it appears that there is no detrimental effect to the performance of a centroid tracker by compensating higher order turbulence from an uncorrelated angle. This is confirmed both by the results from the point source data, and the extended source data. This seems to confirm previous work [13] that shows there is very little correlation between tilt (Zernikes Z_2 and Z_3) and the other Zernike polynomials. This would explain why the tilt variance did not increase appreciably as the higher order adaptive optics beacon moved away from the track target.

Another lesson that can be learned from this research involves the method of determining the level of turbulence. The turbulence levels used for this effort were based on r_0, which was shown to be an inaccurate method for horizontal paths. The strong turbulence affected the performance of the adaptive optics compensation. Additionally, the intensity variations in the images of the both the track beacon and target board would potentially have a detrimental effect on the centroid measurements.

5.2 Potential for Future Research

Several new topics of interest have been explored in this research. These topics present new ideas for future theses.

5.2.1 Compensate the HEL. In order to get the best quality irradiance at the target board, it would be necessary to compensate the outgoing beam for

higher order distortions. This could be accomplished by sending the HEL through another optical phase delay map with the same commands used by the adaptive optics system. It would then be necessary to send the HEL back through the same path that was travelled by the the adaptive optics beacon. This could be accomplished by offsetting the track command by the difference between the track beacon and the adaptive optics beacon, i.e. $\Delta x/L$. This would still allow the pointing to be controlled by the TILL measurements while compensating the outgoing beam.

5.2.2 Feature Track Algorithms. The next logical extension on the project would be to develop a feature tracker and compare the results from that to those from the centroid tracker. Since an edge tracker is much more sensitive to higher order aberrations, it is likely that there would be some pronounced effect on the performance.

5.2.3 Utilizing for Optimal Tracking. If a clear performance degradation is experienced using other tracking techniques, a new design would likely be desirable. This would likely consist of a hybrid of using a compensated path and an uncompensated path. By trading off from one to the other, depending on the turbulence strength and the observed value of θ_0, an adaptive solution could be obtained. Even more desirably the information from both paths could be combined optimally to produce the "best" solution. This would require extensive examination of the cross-correlation properties between the two paths.

Bibliography

1. Air Force Research Laboratory Office of Public Affairs, "North Oscura Peak." http://www.de.afrl.af.mil/factsheets/oscura.html, 1999.
2. Airborne Laser System Program Office, "Airborne Laser (YAL-1A) Fact Sheet." http://www.de.afrl.af.mil/Factsheets/AirborneLaser.html, 2002.
3. Andrews, Larry C. and Ronald L. Phillips. *Laser Beam Propagation through Random Media*. Bellingham, Washington: SPIE Optical Engineering Press, 1998.
4. Coy, Stephen C. "ABLSim: a user-friendly wave optics propagation code." *Airborne Laser Advanced Technology II, SPIE Vol. 3706*. 151–158. 1999.
5. Freeman, R. H., R. J. Freiberg and H. R. Garcia. "Adaptive laser resonator," *Optics Letters*, *2*(3):61–63 (March 1978).
6. Fried, David L. "Anisoplanatism in adaptive optics," *Journal of the Optical Society of America*, *72*(1):52–61 (January 1982).
7. Gardner, C. S., B. M. Welsh and L. A. Thompson. "Design and performance analysis of adaptive optical telescopes using laser guide stars." *Proceedings, IEEE Vol. 78*. 1721–1743. 1990.
8. Goodman, Joseph W. *Introduction to Fourier Optics*. New York: McGraw-Hill, 1996.
9. Hardy, John W. and Richard W. Hudgin. "A Comparison of Wavefront Sensing Systems." *Adaptive Optical Components, SPIE Vol. 141*. 67–72. 1978.
10. Laboratory of the Adaptive Optics for Industrial and Medical Applications, Institute on Laser and Information Technologies, Russian Academy of Sciences, "Shack-Hartmann Wavefront Sensor for Laser Beam Analysis." http://www.laser.ru/adopt/Science/sens/sensor.htm, 2002.
11. MZA Associates Corporation, "WaveTrain, wave optics for the rest of us." http://www.mza.com/wavetrain/, 2001.
12. Noll, Robert J. "Zernike polynomials and atmospheric turbulence," *Journal of the Optical Society of America*, *66*(3):207–211 (March 1976).
13. Roddier, Nicolas. "Atmospheric wavefront simulation and Zernike polynomials." *Amplitude and Intensity Spatial Interferometry, SPIE Vol. 1237*. 668–679. 1990.
14. Roggemann, Michael C. and Byron Welsh. *Imaging Through Turbulence*. Boca Raton, FL: CRC Press LLC, 1996.

15. Tyson, Robert K. *Principles of Adaptive Optics 2nd Edition*. San Diego, CA: Academic Press, 1998.

16. Zetterlind III, Virgil E. *Distributed Beacon Requirements for Branch Point Tolerant Laser Beam Compensation in Extended Atmospheric Turbulence*. MS thesis, Air Force Institute of Technology, Wright-Patterson AFB, OH, March 2002.

Vita

Jason A. Tellez graduated from the United States Air Force Academy in 1996 with a B.S. in Engineering Sciences. He was subsequently assigned to the then Phillips Laboratory at Kirtland Air Force Base, New Mexico, where he worked in the Airborne Laser Technology Branch. In 1999 he was transferred to the National Air Intelligence Center at Wright-Patterson Air Force Base, Ohio, and enrolled in the Air Force Institute of Technology as a part time student graduating in September 2002. Captain Tellez's next assignment is at Detachment 12, Space and Missile Center, Space Vehicles Operations at Kirtland Air Force Base, New Mexico.

REPORT DOCUMENTATION PAGE

Form Approved
OMB No. 074-0188

1. REPORT DATE *(DD-MM-YYYY)*	2. REPORT TYPE	3. DATES COVERED *(From – To)*
01-09-2002	**Master's Thesis**	Mar 2001 – Sep 2002

4. TITLE AND SUBTITLE

HIGH ENERGY LASER POINTING THROUGH EXTENDED TURBULENCE

5a. CONTRACT NUMBER

5b. GRANT NUMBER

5c. PROGRAM ELEMENT NUMBER

6. AUTHOR(S)

Tellez, Jason, A., Captain, USAF

5d. PROJECT NUMBER

5e. TASK NUMBER

5f. WORK UNIT NUMBER

7. PERFORMING ORGANIZATION NAMES(S) AND ADDRESS(S)
Air Force Institute of Technology
Graduate School of Engineering and Management (AFIT/EN)
2950 P Street, Building 640
WPAFB OH 45433-7765

8. PERFORMING ORGANIZATION REPORT NUMBER

AFIT/GE/ENG/02-31

9. SPONSORING/MONITORING AGENCY NAME(S) AND ADDRESS(ES)
AFRL/DEBA
Attn: Mr. Donald Washburn
3550 Aberdeen Ave. SE, Bldg. 401 Rm. 114 DSN: 246-1597
Kirtland AFB, OH 87117-5776 e-mail:
Donald.Washburn@kirtland.af.mil

10. SPONSOR/MONITOR'S ACRONYM(S)

11. SPONSOR/MONITOR'S REPORT NUMBER(S)

12. DISTRIBUTION/AVAILABILITY STATEMENT

APPROVED FOR PUBLIC RELEASE; DISTRIBUTION UNLIMITED.

13. SUPPLEMENTARY NOTES

14. ABSTRACT

The airborne laser (ABL) uses adaptive optics to compensate for the atmospheric turbulence between the ABL and the target. The primary purpose of this compensation is to increase the energy density of the high energy laser at the target. However, the specifics of the engagement scenario require the tracking point of reference and the adaptive optics point of reference to be located at different points on the target.

This research considers the effects of tracking a target in one direction while compensating for atmospheric turbulence in a different direction. The target references used are a point source and a rectangle, while a point source alone is used for the adaptive optics reference. It will be shown that compensating for atmospheric turbulence in a different direction than tracking results in a bias in the mean tracking error while having no appreciable affect on track jitter.

15. SUBJECT TERMS
Adaptive Optics, Anisoplanatism, Optical Tracking, Phase Conjugation, Airborne Laser, Atmospheric Turbulence, Centroid Tracking

16. SECURITY CLASSIFICATION OF:			17. LIMITATION OF ABSTRACT	18. NUMBER OF PAGES	19a. NAME OF RESPONSIBLE PERSON
a. REPORT	b. ABSTRACT	c. THIS PAGE			Eric P. Magee, Maj, USAF (ENG)
U	U	U	UU	67	19b. TELEPHONE NUMBER *(Include area code)* (937) 255-3636, ext 4614; e-mail: Eric.Magee@afit.edu

Standard Form 298 (Rev. 8-98)
Prescribed by ANSI Std. Z39-18